Reverse time shot-geophone migration

William W. Symes [*], *Christiaan C. Stolk* [†], *Biondo Biondi* [‡], *Fuchun Gao* [§]

ABSTRACT

Shot-geophone migration, commonly accomplished using wavefield depth extrapolation ("survey sinking"), has a two way reverse time realization as well. The reverse time version permits imaging of overturned reflections. Shot-geophone migration differs from other prestack migrations in the definition of the prestack image volume which it creates. This difference is most clearly seen by identifying shot-geophone migration as the adjoint of an appropriate forward modeling operator. The offset vector parametrizing shot-geophone image gathers need not be horizontal, and this fact can be used to good effect in constructing prestack images of near-vertical or overturned structures. Unlike other prestack migrations, the image property of shot-geophone migration characteristic of correct velocity - focussing of reflection energy at zero offset - holds in strongly refracting media.

INTRODUCTION

The basis of migration velocity analysis is the *semblance principle*: prestack migrated data volumes contain *flat image gathers*, i.e. are at least kinematically independent of the bin or stacking parameter, when the velocity is correct (Kleyn, 1983; Yilmaz, 1987). Migration velocity analysis (as opposed to standard NMO-based velocity analysis) is most urgently needed in areas of strong lateral velocity variation, i.e. "complex" structure such as salt flanks, chalk tectonics, and overthrust geology. However strong refraction implies multiple raypaths connecting source and receiver locations with reflection points, and multiple raypaths in turn imply that the semblance principle is not valid: that is, image gathers are *not* in general flat, even when the migration velocity closely approximates the true propagation velocity (Stolk and Symes, 2004).

[*]The Rice Inversion Project, Department of Computational and Applied Mathematics, Rice University, Houston TX 77251-1892 USA, email `symes@caam.rice.edu`

[†]Department of Applied Mathematics, University of Twente, Drienerlolaan 5, 7522 NB Enschede, The Netherlands, email `c.c.stolk@ewi.utwente.nl`

[‡]Stanford Exploration Project, Department of Geophysics, Stanford University, Stanford CA 94305-2215 USA, email `biondo@sep.stanford.edu`

[§]The Rice Inversion Project, Department of Earth Sciences, Rice University, Houston TX 77251-1892 USA, email `fcgao@esci.rice.edu`

The failure of the semblance principle in complex structure afflicts all prestack migration techniques based on data binning, i.e. for which each data bin creates an independent image. This category includes many variants of common shot, common offset and common scattering angle migration - see (Nolan and Symes, 1996; Nolan and Symes, 1997; Xu et al., 2001; Prucha et al., 1999; Stolk, 2002; Stolk and Symes, 2004). However one well-known form of prestack image formation does *not* migrate image bins independently: this is Claerbout's *survey-sinking migration* (Claerbout, 1985), commonly implemented using some variety of one-way wave equation to extrapolate source and receiver depths. The semblance principle for survey sinking migration differs from that appropriate to other prestack migrations: rather than being flat in offset, energy is *focussed* at zero offset when the velocity is kinematically correct. This paper refers to this variant of the semblance principle as the *focussing property*.

Note that survey sinking migration is limited to migration velocity model - data combinations in which rays carrying significant energy travel essentially vertically (the "DSR condition", per (Stolk and De Hoop, 2001)).

Recently (Stolk and De Hoop, 2001) showed that survey sinking does *not* create image artifacts, i.e. that the focussing property holds in media of essentially arbitrary complexity, provided that the DSR condition is valid. Stolk and deHoop also showed that a "Kirchhoff" or diffraction sum implementation is possible, which makes it clear that depth extrapolation *per se* is not the explanation for the good semblance (focussing) property of survey sinking migration. The basis of this ray theoretic analysis is a DSR forward modeling operator, of which the survey-sinking migration operator is the adjoint.

Once one understands survey-sinking migration as the adjoint operator of a shot-geophone model, it is clear that this migration is a special case of a general class of *shot-geophone migration methods*, and that these can be formulated without reference to one-way wavefield extrapolation. The purpose of this paper is to introduce this more general family of migration operators, describe two-way reverse time methods for computing them, and to establish their artifact-free nature. We give a different and somewhat simpler argument than the one in (Stolk and De Hoop, 2001) for the absence of kinematic artifacts under the DSR hypothesis. In contrast to (Claerbout, 1985; Stolk and De Hoop, 2001), our formulation and analysis accomodates *non-horizontal offset*, and we explain the importance of this generalization for imaging near-vertical or overturned structure. Imaging of reflectors at arbitrary angle of dip requires that the dip vector not be parallel to the direction of offset - otherwise the focussing property is lost, for example in attempting to image a vertical reflector using only horizontal offsets in shot-geophone migration. We illustrate this phenomenon with simple examples, and explain it via ray theory.

For the general (non-DSR) case we propose a method for imaging all dips simultaneously by combining two or more depth offset directions, with appropriate midpoint dip filtering. In this case, the focussing property cannot in general be guaranteed in the simple form for which it holds when the DSR condition is satisfied. Instead, we show that image volume energy is localized (i) at zero offset, and (ii) possibly outside a corridor around zero offset. We relate the width of the corridor to properties of the ray fields, which are

necessary for a final stacked image at correct velocity to faithfully render the reflectors in the subsurface (traveltime injectivity condition, no scattering over π).

The papers (Biondi and Shan, 2002; Biondi and Symes, 2004) introduce essentially the same family of reverse time algorithms, along with the notion of general (non-horizontal) subsurface offset. These papers shows that shot-geophone reverse time migration retains the property which has led in the past to interest in reverse time migration (Whitmore, 1983; Yoon et al., 2003): it images reflectors which are invisible to depth extrapolation migration due to overturned raypaths. The approach to imaging all dips proposed in (Biondi and Symes, 2004) produces a single angle domain volume, rather than the three offset domain volumes (one for each coordinate axis) proposed here. The input to the angle domain image construction is essentially the three image volumes defined in this paper, however, and the two approaches are very closely related. The concept of *geological dip* is central to the definition of image gather developed in (Biondi and Symes, 2004). In the present paper, we develop an alternate definition of shot-geophone image volume whose focussing properties do not depend on a well-defined geologic dip. Since geologic dip may be ill-defined at important locations within the sedimentary section, eg. at pinchouts and salt truncations, we believe this alternate construction to be potentially useful.

TWO WAY SHOT-GEOPHONE MIGRATION

This section introduces shot-geophone migration as the adjoint of a shot-geophone modeling operator, with a completely general offset vector. The paper (Stolk and De Hoop, 2001) shows how Claerbout's survey sinking migration *via* DSR extrapolation arises as a special case.

We assume that sources and receivers lie on the same depth plane, and adjust the depth axis so that the source-receiver plane is $z = 0$. This restriction is can be removed at the cost of more complicated notation (and numerics): it is not essential. Nothing about the formulation of the migration method presented below *requires* that data be given on the full surface $z = 0$.

While the examples to be presented later are all 2D, the construction is not: in the following $\mathbf{x}$ (and other bold face letters) will denote either two- or three-dimensional vectors. Source locations are $\mathbf{x}_s$, receiver locations are $\mathbf{x}_r$.

Single scattering

The causal acoustic Green's function $G(\mathbf{x}, t; \mathbf{x}_s)$ for a point source at $\mathbf{x} = \mathbf{x}_s$ is the solution of

$$\frac{1}{v^2(\mathbf{x})}\frac{\partial^2 G}{\partial t^2}(\mathbf{x}, t; \mathbf{x}_s) - \nabla^2_{\mathbf{x}} G(\mathbf{x}, t; \mathbf{x}_s) = \delta(\mathbf{x} - \mathbf{x}_s)\delta(t) \tag{1}$$

with $G = 0, t < 0$.

In common with all other migration methods, shot-geophone migration is based on the Born or single scattering approximation. Denote by $r(\mathbf{x}) = \delta v(\mathbf{x})/v(\mathbf{x})$ a relative

perturbation of the velocity field. Then linearization of the wave equation yields for the corresponding perturbation of the Green's function

$$\frac{1}{v^2(\mathbf{x})}\frac{\partial^2 \delta G}{\partial t^2}(\mathbf{x},t;\mathbf{x}_s) - \nabla^2_{\mathbf{x}}\delta G(\mathbf{x},t;\mathbf{x}_s) = \frac{2r(\mathbf{x})}{v^2(\mathbf{x})}\frac{\partial^2}{\partial t^2}G(\mathbf{x},t;\mathbf{x}_s) \tag{2}$$

whose solution has the integral representation at the source and receiver points $\mathbf{x}_r, \mathbf{x}_s$

$$\delta G(\mathbf{x}_r,t;\mathbf{x}_s) = \frac{\partial^2}{\partial t^2}\int dx \int dh \int d\tau \frac{2r(\mathbf{x})}{v^2(\mathbf{x})}G(\mathbf{x},t-\tau;\mathbf{x}_r)G(\mathbf{x},\tau;\mathbf{x}_s) \tag{3}$$

The singly scattered field is the time convolution of δG with a source wavelet (or the space-time convolution with a radiation pattern operator, for more complex sources). Since the principal concern of this paper is kinematic relationships between data and image, we will ignore the filtering by the source signature (i.e. replace it with a delta function). This effective replacement of the source by an impulse does not seem to invalidate the predictions of the theory, though the matter is certainly worthy of more study.

Thus the Born modeling operator $F[v]$ is

$$F[v]r(\mathbf{x}_r,t;\mathbf{x}_s) = \delta G(\mathbf{x}_r,t;\mathbf{x}_s)$$

Prestack shot profile modeling results from replacing $2r(\mathbf{x})/v^2(\mathbf{x})$ with $R(\mathbf{x},\mathbf{x}_s)$, i.e. permitting reflectivity to be defined differently for each shot. Examination of equation (2) shows that each shot is then modeled independently of every other. The adjoint of the shot profile modeling operator is shot profile migration; since Born modeling is just shot profile modeling with $R(\mathbf{x},\mathbf{x}_s) = 2r(\mathbf{x})/v^2(\mathbf{x})$, Born migration is shot profile migration followed by the adjoint of the "spray" mapping $r(\mathbf{x}) \mapsto R(\mathbf{x},\mathbf{x}_s) = 2r(\mathbf{x})/v^2(\mathbf{x})$, which is the stack. The other standard prestack migrations via data binning have similar relationships to Born migration.

Shot-geophone modeling and migration in midpoint-offset coordinates

Shot-geophone modeling results from a different generalization of reflectivity: replace $2r(\mathbf{x})/v^2(\mathbf{x})$ by $R(\mathbf{x},\mathbf{h})$ where $\mathbf{h}$ is the depth (half)offset mentioned in the introduction. The coordinate $\mathbf{x}$ plays the role of midpoint.

Remark: If the velocity is constant, at least locally in a region to be imaged, it is possible to interpret the midpoint $\mathbf{x}$ as an image point (Biondi and Symes, 2004). In general this is not possible, and only the offset coordinate $\mathbf{h}$ has direct physical significance.

Replace the Born scattering field δG by the field u, defined by equation (3) by

$$u(\mathbf{x}_r,t;\mathbf{x}_s) = \frac{\partial^2}{\partial t^2}\int dx \int dh \int d\tau\, R(\mathbf{x},\mathbf{h})G(\mathbf{x}+\mathbf{h},t-\tau;\mathbf{x}_r)G(\mathbf{x}-\mathbf{h},\tau;\mathbf{x}_s) \tag{4}$$

It is easy to see that $u(\mathbf{x}_r, t; \mathbf{x}_s)$ is the value at $\mathbf{y} = \mathbf{x}_r$ of the modified shot-profile field $u(\mathbf{y}, t; \mathbf{x}_s)$, which solves

$$\frac{1}{v^2(\mathbf{y})}\frac{\partial^2 u}{\partial t^2}(\mathbf{y}, t; \mathbf{x}_s) - \nabla^2_{\mathbf{y}} u(\mathbf{y}, t; \mathbf{x}_s) = \int dh\, R(\mathbf{y} - \mathbf{h}, \mathbf{h})\frac{\partial^2}{\partial t^2}G(\mathbf{y} - 2\mathbf{h}, t; \mathbf{x}_s) \tag{5}$$

The shot-geophone modeling operator $\bar{F}[v]$ is given by

$$\bar{F}[v]R(\mathbf{x}_r, t; \mathbf{x}_s) = u(\mathbf{x}_r, t; \mathbf{x}_s)$$

The field $u(\mathbf{x}, t; \mathbf{x}_s)$ is identical to $\delta G(\mathbf{x}, t; \mathbf{x}_s)$ when

$$R(\mathbf{x}, \mathbf{h}) = \frac{2r(\mathbf{x})}{v^2(\mathbf{x})}\delta(\mathbf{h})$$

i.e. when the generalized reflectivity is concentrated at offset zero. Therefore Born modeling is shot-geophone modeling following the mapping

$$r(\mathbf{x}) \mapsto \frac{2r(\mathbf{x})}{v^2(\mathbf{x})}\delta(\mathbf{h}) \tag{6}$$

Born migration is then shot-geophone migration followed by the adjoint of the mapping defined in equation (6), i.e. which is

$$R(\mathbf{x}, \mathbf{h}) \mapsto \frac{2R(\mathbf{x}, 0)}{v^2(\mathbf{x})} \tag{7}$$

i.e. shot-geophone migration followed by extraction off the zero offset section.

The shot-geophone migration operator is the adjoint of the shot-geophone modeling operator. Its reverse time implementation is a minor variation on the usual implementation of reverse time migration (the "adjoint state method", see eg. (Tarantola, 1987; Whitmore, 1983; Lailly, 1983; Yoon et al., 2003)). We give a derivation in Appendix A, for the sake of completeness. The result is

$$\bar{F}^*[v]d(\mathbf{x}, \mathbf{h}) = -\int dx_s \int_0^T dt\, \frac{\partial q}{\partial t}(\mathbf{x} + \mathbf{h}, t; \mathbf{x}_s)\frac{\partial^2 G}{\partial t^2}(\mathbf{x} - \mathbf{h}, t; \mathbf{x}_s) \tag{8}$$

where the *adjoint state* or backpropagated field $q(\mathbf{x}, t; \mathbf{x}_s)$ satisfies $q \equiv 0$, $t \geq T$ and

$$\left(\frac{1}{v(\mathbf{x})^2}\frac{\partial^2}{\partial t^2} - \nabla^2_{\mathbf{x}}\right) q(\mathbf{x}, t; \mathbf{x}_s) = \int dx_r\, d(\mathbf{x}_r, t; \mathbf{x}_s)\delta(\mathbf{x} - \mathbf{x}_r) \tag{9}$$

Remark: Note that the backpropagated field is *not* in general the physical scattered field, time-reversed. It is a mathematical convenience which permits a simple computation of the adjoint, with no immediate physical significance. Discretization of the wave equation for the scattered field (2), eg. by finite differences, gives a linear system, written implicitly as a recursion. The calculation specified by equations (8,9) is the continuous limit of the transposed system, again written implicitly as a recursion.

The migration operator defined by equations (8,9) is very similar to the usual prestack reverse time migration operator:

1. The adjoint state field q is *exactly* the same as the usual adjoint state field which appears in two-way reverse time migration, i.e. the solution of the problem (9), and is computed independently for each shot;

2. The Green's function $G(\mathbf{x}, t; \mathbf{x}_s)$ is *exactly* the same reference field used in shot profile two way reverse time migration, i.e. the solution of the problem (1), and can also be computed shot-by-shot;

3. The imaging condition (8) is *exactly* the same as the usual two-way reverse time shot profile imaging condition when $\mathbf{h} = 0$; the latter is the reverse time version of Claerbout's survey-sinking imaging condition (Claerbout, 1985).

4. Therefore the only real difference with standard two way reverse time migration comes in the $\mathbf{h}$ dependence in (8), which implies a loop over $\mathbf{h}$. Note that this does not require the solution of any new PDEs: it simply inserts a new loop in the computation of the adjoint image (migration output), over $\mathbf{h}$. Thus the image can still be accumulated in a loop over shots of independent, shot-by-shot computations, exactly as is done in standard reverse time migration. The additional computational burden of the $\mathbf{h}$ loop depends on the sampling and range of $\mathbf{h}$, and on the proportion of the maximum possibly image volume computed. This proportion may be small: velocity analysis typically requires only a small fraction of the possible image gathers. We will return to this issue briefly in the discussion section.

Shot-geophone modeling and migration in source-receiver coordinates

It turns out to be convenient to introduce a more symmetrical representation of shot-geophone modeling, which we dub the *source-receiver representation*.

Define coordinates $\mathbf{y}_s = \mathbf{x} - \mathbf{h}$, $\mathbf{y}_r = \mathbf{x} + \mathbf{h}$; these will turn out to be coordinates along rays from source and receiver respectively. Define the *source-receiver reflectivity* $\bar{R}$ by

$$\bar{R}(\mathbf{y}_s, \mathbf{y}_r) = R\left(\frac{\mathbf{y}_s + \mathbf{y}_r}{2}, \frac{\mathbf{y}_r - \mathbf{y}_s}{2}\right), \text{ i.e. } \bar{R}(\mathbf{x} - \mathbf{h}, \mathbf{x} + \mathbf{h}) = R(\mathbf{x}, \mathbf{h})$$

Then change integration variables in equation (4)

$$\bar{F}[v]\bar{R}(\mathbf{x}_r, t; \mathbf{x}_s) = \frac{1}{2}\frac{\partial^2}{\partial t^2} \int dy_s \int dy_r \int d\tau\, \bar{R}(\mathbf{y}_s, \mathbf{y}_r) G(\mathbf{y}_r, t - \tau; \mathbf{x}_r) G(\mathbf{y}_s, \tau; \mathbf{x}_s) \quad (10)$$

It follows that

$$F[v]R(\mathbf{x}_r, t; \mathbf{x}_s) = \bar{F}[v]\bar{R}(\mathbf{x}_r, t; \mathbf{x}_s) = u(\mathbf{x}_r, t; \mathbf{x}_s)$$

where u solves both

$$\frac{1}{v^2(\mathbf{x})}\frac{\partial^2 u}{\partial t^2}(\mathbf{x}, t; \mathbf{x}_s) - \nabla^2_{\mathbf{x}} u(\mathbf{x}, t; \mathbf{x}_s) = \int dy_s\, \bar{R}(\mathbf{y}_s, \mathbf{x}) \frac{\partial^2}{\partial t^2} G(\mathbf{y}_s, t; \mathbf{x}_s) \quad (11)$$

and

$$\frac{1}{v^2(\mathbf{x})}\frac{\partial^2 u}{\partial t^2}(\mathbf{x}_r, t; \mathbf{x}) - \nabla^2_{\mathbf{x}} u(\mathbf{x}_r, t; \mathbf{x}) = \int dy_r\, \bar{R}(\mathbf{x}, \mathbf{y}_r) \frac{\partial^2}{\partial t^2} G(\mathbf{y}_r, t; \mathbf{x}_r) \quad (12)$$

The source-receiver representation of shot-geophone migration is

$$\bar{F}[v]^* d(\mathbf{y}_s, \mathbf{y}_r) = \int dx_s \int dt q(\mathbf{y}_r, t; \mathbf{x}_s) \frac{\partial^2}{\partial t^2} G(\mathbf{y}_s, t; \mathbf{x}_s) \tag{13}$$

in which q is the backpropagated field described in the last subsection (solution of equation (9)). Note that the imaging condition (13) collapses to the usual imaging condition when $\mathbf{y}_s$ and $\mathbf{y}_r$ concide with an image point (zero offset).

Remark: The source-receiver representation is important for the kinematic analysis to follow. However the midpoint-offset representation is more convenient for computation.

Kirchhoff representation of shot-geophone migration

An integral or "Kirchhoff" representation of the shot-geophone migration operator is also possible. We mention this here to emphasize that the computational representation of the shot-geophone migrated field is not the determinant of its favorable kinematic properties: two way reverse time, Kirchhoff, and depth extrapolation computations will yield equivalent migrations, within the domain of validity of each. The Kirchhoff representation described here is in principle kinematically equivalent to two-way reverse time computation, as described in the previous subsection. Depth extrapolation computations have a more restricted domain of validity.

Application of standard high frequency asymptotics and stationary phase arguments to the integral representation of the shot-geophone field (3) gives

$$F[v]R(\mathbf{x}_r, t; \mathbf{x}_s) = \frac{\partial^2}{\partial t^2} \sum_{i,j} \int \int dx\, dh\, A^{(i,j)}(\mathbf{x}, \mathbf{h}, \mathbf{x}_s, \mathbf{x}_r)\, \delta(t - T^{(i,j)}(\mathbf{x}, \mathbf{h}, \mathbf{x}_s, \mathbf{x}_r)) R(\mathbf{x}, \mathbf{h}) \tag{14}$$

in which $T^{(i,j)}(\mathbf{x}, \mathbf{h}, \mathbf{x}_s, \mathbf{x}_r)$ is the sum of the ith branch of the (one-way) traveltime from the source point $\mathbf{x}_s$ to the source-ray scattering point $\mathbf{x} - \mathbf{h}$, and the jth branch of the traveltime from the receiver-ray scattering point $\mathbf{x} + \mathbf{h}$ to the receiver point $\mathbf{x}_r$, and $A^{(i,j)}(...)$ is an amplitude involving spreading factors, velocity, etc. (Stolk and Symes, 2004). The Kirchhoff shot-geophone migration formula is then

$$F^*[v]d(\mathbf{x}, \mathbf{h}) \simeq \int \int dx_s dx_r \sum_{i,j} A^{(i,j)}(\mathbf{x}, \mathbf{h}, \mathbf{x}_s, \mathbf{x}_r) \frac{\partial^2 d}{\partial t^2}(\mathbf{x}_s, \mathbf{x}_r, T^{(i,j)}(\mathbf{x}, \mathbf{h}, \mathbf{x}_s, \mathbf{x}_r)) \tag{15}$$

These formulas were derived in a different way in (Stolk and De Hoop, 2001) for the special case $h_3 = 0$, i.e. horizontal depth-offset, and used to analyze the kinematics of shot-geophone migration, to which we now turn.

KINEMATICS OF SHOT-GEOPHONE MIGRATION

An event in the data is characterized by its (3D) moveout: locally, by a moveout equation $t = T(\mathbf{x}_s, \mathbf{x}_r)$, and infinitesimally by the source and receiver slownesses

$$\mathbf{p}_s = \nabla_{\mathbf{x}_s} T, \ \mathbf{p}_r = \nabla_{\mathbf{x}_r} T$$

Significant energy with this moveout implies that locally near $(\mathbf{x}_s, \mathbf{x}_r, t)$ the data contains a plane wave component with wavenumber $(\omega\mathbf{p}_s, \omega\mathbf{p}_r, \omega)$. These coordinates (position, wavenumber) give the phase space representation of the event.

Note that for incomplete coverage, eg. marine streamer geometry, an event in the data will not determine its (3D) moveout uniquely. For example, in (idealized) marine streamer geometry, with the streamers oriented along the x axis, the y component of $\mathbf{p}_r$ is not determined by the data. In the discussion to follow, $\mathbf{p}_s$ and $\mathbf{p}_r$ are assumed to be *compatible* with a data event.

Likewise, a reflector (in the source-receiver representation) at $(\mathbf{y}_s, \mathbf{y}_r)$ with wavenumber $(\mathbf{k}_s, \mathbf{k}_r)$ is characterized in (image volume) phase space by these coordinates.

The kinematical description of shot-geophone migration relates the phase space coordinates of events and reflectors. An event with phase space representation

$$(\mathbf{x}_s, \mathbf{x}_r, t_{sr}, \omega\mathbf{p}_s, \omega\mathbf{p}_r, \omega)$$

is the result of a reflector with (double reflector) phase space representation $(\mathbf{y}_s, \mathbf{y}_r, \mathbf{k}_s, \mathbf{k}_r)$ exactly when

- there is a ray $(\mathbf{X}_s, \mathbf{P}_s)$ leaving the source point $\mathbf{X}_s(0) = \mathbf{x}_s$ at time $t = 0$ with ray parameter $\mathbf{P}_s(0) = \mathbf{p}_s$, and arriving at $\mathbf{X}_s(t_s) = \mathbf{y}_s$ at $t = t_s$ with ray parameter $\mathbf{P}_s(t_s) = -\mathbf{k}_s/\omega$;
- there is a ray $(\mathbf{X}_r, \mathbf{P}_r)$ leaving $\mathbf{X}_r(t_s) = \mathbf{y}_r$ at $t = t_s$ with ray parameter $\mathbf{P}_r(t_s) = \mathbf{k}_r/\omega$ and arriving at the receiver point $\mathbf{X}_r(t_{sr}) = \mathbf{x}_s$ at time $t = t_{sr} = t_s + t_r$ with ray parameter $\mathbf{P}_r(t_{sr}) = \mathbf{p}_r$.

Figure 1 illustrates this kinematic relation. Appendix B provides a derivation.

Note that since $\mathbf{P}_s, \mathbf{P}_r$ are ray slowness vectors, there is necessarily a length relation between $\mathbf{k_s}, \mathbf{k_r}$: namely,

$$\frac{1}{v(\mathbf{y}_s)} = \|\mathbf{P}_s(t_s)\| = \frac{\|\mathbf{k_s}\|}{|\omega|}$$
$$\frac{1}{v(\mathbf{y}_r)} = \|\mathbf{P}_r(t_r)\| = \frac{\|\mathbf{k_r}\|}{|\omega|}$$

whence

$$\frac{\|\mathbf{k_r}\|}{\|\mathbf{k_s}\|} = \frac{v(\mathbf{y}_s)}{v(\mathbf{y}_r)} \tag{16}$$

The kinematics of shot-geophone migration are somewhat strange, so it is reassuring to see that for physical reflectors (i.e. $\bar{R}(\mathbf{y}_s, \mathbf{y}_r) = r(\mathbf{x})\delta(\mathbf{h})$) the relation just explained becomes the familiar one of reflection from a reflecting element according to Snell's law. A quick calculation shows that such a physical $\bar{R}$ has a significant local plane wave component near $(\mathbf{y}_s, \mathbf{y}_r)$ with wavenumber $(\mathbf{k}_s, \mathbf{k}_r)$ only if $\mathbf{y}_s = \mathbf{y}_r = \mathbf{x}$ and r has a significant local plane wave component near $\mathbf{x}$ with wavenumber $\mathbf{k}_x = \mathbf{k}_s + \mathbf{k}_r$. From equation (16),

$\mathbf{k}_s$ and $\mathbf{k}_r$ have the same length, therefore their sum $\mathbf{k}_x$ is also their bisector, which establishes Snell's law. Thus a single (physical) reflector at $\mathbf{x}$ with wavenumber ξ gives rise to a reflected event at frequency ω exactly when the rays $(\mathbf{X}_s, \mathbf{P}_s)$ and $(\mathbf{X}_r, \mathbf{P}_r)$ meet at $\mathbf{x}$ at time t_s, and the reflector dip $\mathbf{k}_x = \omega(\mathbf{P}_r(t_s) - \mathbf{P}_s(t_s))$, which is the usual kinematics of single scattering. See Figure 2.

It is now possible to answer the question: in the shot-geophone model, to what extent does a data event determine the corresponding reflector? The rules derived above show that the reflection point $(\mathbf{y}_s, \mathbf{y}_r)$ must lie on the Cartesian product of two rays, $(\mathbf{X}_s, \mathbf{P}_s)$ and $(\mathbf{X}_r, \mathbf{P}_r)$, consistent with the event, and the total time is also determined. If the coverage is complete, so that the event uniquely determines the source and receiver rays, then the source-receiver representation of the source-receiver reflector must lie along this uniquely determined ray pair. This fact contrasts dramatically with the imaging ambiguities demonstrated in (Nolan and Symes, 1996; Nolan and Symes, 1997; Xu et al., 2001; Prucha et al., 1999; Stolk, 2002; Stolk and Symes, 2004) for all forms of prestack depth migration based on data binning. Even when coverage is complete, in these other forms of prestack migration strong refraction leads to multiple ray pairs connecting data events and reflectors, whence ambiguous imaging of a single event in more than one location within the prestack image volume.

Nonetheless reflector location is still not uniquely determined by shot-geophone migration as defined above, for two reasons:

- Only the total traveltime is specified by the event! Thus if $\mathbf{y}_s = \mathbf{X}_s(t_s), \mathbf{y}_r = \mathbf{X}_r(t_s)$ are related as described above to the event determining the ray pair, so is $\mathbf{y}'_s = \mathbf{X}_s(t'_s), \mathbf{y}'_r = \mathbf{X}_r(t'_s)$ with $t_s + t_r = t'_s + t'_r = t_{sr}$. See Figure 1.
- Incomplete coverage may prevent the event from determining its 3D moveout, as mentioned above, and therefore a family of ray pairs, rather than a unique ray pair, corresponds to the event.

KINEMATICS WITH RESTRICTED OFFSETS

One way to view the remaining imaging ambiguity in shot-geophone migration as defined so far is to recognize that the image point coordinates $(\mathbf{y}_s, \mathbf{y}_r)$ (or $(\mathbf{x}, \mathbf{h})$) are six-dimensional (in 3D), whereas the data depends on only five coordinates $(\mathbf{x}_r, t, \mathbf{x}_s)$ (at most). Formally, restricting one of the coordinates of the image point to be zero would at least make the variable counts equal, so that unambiguous imaging would at least be conceivable. Since physical reflectivities are concentrated at zero (vector) offset, it is natural to restrict one of the offset coordinates to be zero.

Imaging conditions with restricted offsets

In 3D, there are three possibilities, in which $R(\mathbf{x}, \mathbf{h})$ takes one of the three forms

$$R_x(\mathbf{x}, h_y, h_z)\delta(h_x),\ R_y(\mathbf{x}, h_x, h_z)\delta(h_y),\ R_z(\mathbf{x}, h_x, h_y)\delta(h_z)$$

leading to three restricted modeling operators:

$$\bar{F}_x[v]R_x(\mathbf{x}_r,t;\mathbf{x}_s) = \frac{\partial^2}{\partial t^2}\int dx \int dh_y \int dh_z \int d\tau$$
$$R_x(\mathbf{x},h_y,h_z)G(\mathbf{x}+(0,h_y,h_z),t-\tau;\mathbf{x}_r)G(\mathbf{x}-(0,h_y,h_z),\tau;\mathbf{x}_s) \tag{17}$$
$$\bar{F}_y[v]R_y(\mathbf{x}_r,t;\mathbf{x}_s) = \frac{\partial^2}{\partial t^2}\int dx \int dh_x \int dh_z \int d\tau$$
$$R_x(\mathbf{x},h_x,h_z)G(\mathbf{x}+(h_x,0,h_z),t-\tau;\mathbf{x}_r)G(\mathbf{x}-(h_x,0,h_z),\tau;\mathbf{x}_s) \tag{18}$$
$$\bar{F}_z[v]R_z(\mathbf{x}_r,t;\mathbf{x}_s) = \frac{\partial^2}{\partial t^2}\int dx \int dh_x \int dh_y \int d\tau$$
$$R_x(\mathbf{x},h_x,h_y)G(\mathbf{x}+(h_x,h_y,0),t-\tau;\mathbf{x}_r)G(\mathbf{x}-(h_x,h_y,0),\tau;\mathbf{x}_s) \tag{19}$$

The kinematics of these restricted operators follows directly from that of the unrestricted operator, developed in the preceding section.

Denote $\mathbf{y}_s = (x_s, y_s, z_s), \mathbf{k}_s = (k_{s,x}, k_{s,y}, k_{s,z})$ etc. For restricted x offset,

$$\bar{R}(\mathbf{y}_s,\mathbf{y}_r) = \bar{R}_x\left(\frac{x_s+x_r}{2}, y_s, y_r, z_s, z_r\right)\delta(x_s-x_r)$$

Fourier transformation shows that $\bar{R}$ has a significant plane wave component with wavenumber $(\mathbf{k}_s,\mathbf{k}_r)$ precisely when $\bar{R}_x$ has a significant plane wave component with wavenumber $(k_{s,x}+k_{r,x}, k_{s,y}, k_{x,z}, k_{r,y}, k_{r,z})$. Thus a ray pair $(\mathbf{X}_s,\mathbf{P}_s),(\mathbf{X}_r,\mathbf{P}_r)$ compatible with a data event with phase space coordinates $(\mathbf{x}_r,\mathbf{x}_s,t_{sr},\omega\mathbf{p}_s,\omega\mathbf{p}_r,\omega)$ images at a point $(x,y_s,y_r,z_s,z_r,k_x,k_{s,y},k_{s,z},k_{r,y},k_{r,z})$ provided that for $0\le t_s\le t_sr$, $X_{s,x}(t_s)=X_{r,x}(t_s)=x$, $X_{s,y}(t_s)=y_s$, $X_{r,z}(t_s)=z_s$, $X_{r,y}(t_s)=y_r$, $X_{r,z}(t_s)=z_r$, $P_{r,x}(t_s)-P_{s,x}(t_s)=k_s/\omega$, $P_{s,y}(t_s)=k_{s,y}/\omega$, etc.

Similarly, for restricted y offset,

$$\bar{R}(\mathbf{y}_s,\mathbf{y}_r) = \bar{R}_y\left(x_s, x_r, \frac{y_s+y_r}{2}, z_s, z_r\right)\delta(y_s-y_r)$$

and the imaging conditions are $X_{s,y}(t_s)=X_{r,y}(t_s)=y$, $P_{r,y}(t_s)-P_{s,y}(t_s)=k_s/\omega$, $X_{s,x}(t_s)=x_s$, $P_{s,x}(t_s)=k_{s,x}/\omega$, etc. at image phase space point

$$(x_s,x_r,y,z_s,z_r,k_{s,x},k_{r,x},k_y,k_{s,z},k_{r,z}).$$

For restricted z offset,

$$\bar{R}(\mathbf{y}_s,\mathbf{y}_r) = \bar{R}_z\left(x_s, x_r, y_s, y_r, \frac{z_s+z_r}{2}\right)\delta(z_s-z_r)$$

and the imaging conditions are $X_{s,z}(t_s)=X_{r,z}(t_s)=z$, $P_{r,z}(t_s)-P_{s,z}(t_s)=k_z/\omega$, $X_{s,x}(t_s)=x_s$, $P_{s,x}(t_s)=k_{s,x}/\omega$, etc. at image phase space point

$$(x_s,x_r,y_s,y_r,z,k_{s,x},k_{r,x},k_{s,y},k_{r,y},k_z).$$

Horizontal offset and the DSR condition

As explained in (Stolk and De Hoop, 2001), Claerbout's survey sinking migration is kinematically equivalent to shot-geophone migration as defined here, under two assumptions:

- offsets are restricted to horizontal ($h_z = 0$);
- rays (either source or receiver) carrying significant energy do not turn, i.e. $P_{s,z} > 0, P_{r,z} < 0$ throughout the propagation.

We call the second condition the "Double Square Root", or "DSR", condition, for reasons explained in (Stolk and De Hoop, 2001). This reference also offers a proof of the

Claim: Under these restrictions, the imaging operator $\bar{F}_z$ can image a ray pair at precisely one location in image volume phase space. When the velocity is correct, the image energy is therefore concentrated at zero offset.

The demonstration presented in (Stolk and De Hoop, 2001) uses oscillatory integral representations of the operator $\bar{F}_z$ and its adjoint. However, the conclusion also follows directly from the kinematic analysis above and the DSR condition.

Indeed, note that the DSR condition implies that depth is increasing along the source ray, and decreasing along the receiver ray - otherwise put, depth is increasing along both rays, if you traverse the receiver ray *backwards*. Therefore depth can be used to parametrize the rays. With depth as the parameter, time is increasing from zero along the source ray, and decreasing from t_{sr} along the receiver ray (traversed backwards). Thus the two times can be equal (to t_s) at exactly one point.

Since the scattering time t_s is uniquely determined, so are all the other phase space coordinates of the rays. If the ray pair is the incident-reflected ray pair of a reflector, then the reflector must be the *only* point at which the rays cross, since there is only one time t_s at which $X_{s,z}(t_s) = X_{r,z}(t_s)$. See Figure 3. Therefore in the infinite frequency limit the energy of this incident-reflected ray pair is imaged at zero offset, consistent with Claerbout's imaging condition.

If furthermore coverage is complete, whence the data event uniquely determines the rays, then it follows that a data event is imaged at precisely one location, namely the reflector which caused it, and in particular focusses at zero offset. This is the result established in (Stolk and De Hoop, 2001), for which we have now given a different (and more elementary) proof.

Remark: Note that the DSR assumption precludes the imaging or near- or post-vertical reflectors, since in general for such reflectors it will not be possible to satisfy the imaging conditions without either incident or reflected ray turning horizontal at some point.

Figure 4 illustrates the focussing property and suggests its possible utility for velocity analysis. The data used to generate these migrated image gathers is 2D finite difference synthetic Born data, with a constant background velocity and 2D random reflectivity r. One hundred source positions spaced every 10 m on the surface. The receiver array

is fixed, occupying the same positions as the source. The resulting 10000 traces were migrated, i.e. the adjoint of $\bar{F}_z$ applied, using the method described above (based on equation (8)) with backpropagation carried out via a compatible finite difference method and the crosscorrelation by the trapezoidal rule on the finite difference grid. The figure shows horizontal offset CIGs for the correct velocity, i.e. that used to generate the data, on the left, 10% high velocity in the center, and 10% low velocity on the right. The CIG is well-focussed at the correct velocity; energy spreads to non-zero offsets with deviation from correct velocity.

A second 2D synthetic example emphasizes the dramatic contrast, revealed by the Stolk-deHoop theorem, between the behaviour of shot-geophone migration and other forms of prestack migration. This example is used in (Stolk, 2002; Stolk and Symes, 2004) to show that common offset and Kirchhoff common scattering angle migration generally produce strong kinematic artifacts in strongly refracting velocity models. The velocity model consists of a slow Gaussian lens embedded in a constant background. As shown in Figure 5, this model is strongly refracting - it produces triplications in rayfields shot from surface points - while still obeying the DSR condition, for the offsets used in the example. Below the lens, at a depth of 2 km, we placed a flat reflector. We synthesized data using a (4, 10, 20, 40) zero phase bandpass filter as (isotropic) source wavelet and a finite difference scheme with adequate sampling. A typical shot gather (Figure 6) shows the compex pattern of reflections from the flat reflector propagated through the lens.

We migrated this data using a depth-extrapolation scheme ((Prucha et al., 1999) and references cited there). Figure 11 shows the image (left), a horizontal offset CIG (center), and an angle domain CIG (right, see discussion below). The central panel clearly shows the absence of any violation of the focussing property: all energy is concentrated at zero offset.

Contrast this behaviour with that of Kirchhoff common offset and common scattering angle migration, Figures 7, 8 reproduced from (Stolk and Symes, 2004). For these prestack migration methods, defined by surface binning of the data, image gathers should be flat when correct migration velocity is used (as opposed to focussed at zero offset, as for shot-geophone migration). Instead, numerous highly energetic non-flat events contaminate the gathers. Missing rays are not the cause: all arrivals are used in these computations, with correct phase shifts and amplitudes in the imaging formulae. In fact, these events are kinematic in nature: that is, they cannot be removed by more sophisticated signal processing, but are intrinsic to the ray geometry of these migration methods. See (Stolk and Symes, 2004) for a detailed explanation.

Remark: Note that Kirchhoff common scattering angle migration, as used to produce the gather displayed in Figure 8, is fundamentally different from the angle domain migrations described in (Prucha et al., 1999; Rickett and Sava, 2002; Sava and Fomel, 2003). The former uses an implicit surface-oriented phase space binning of the data, whereas the latter amounts to a Radon transform of the shot-geophone migration output in depth and offset (or is closely related to this transform). The focussing property of shot-geophone migration, just illustrated, implies that angle domain migration also produces artifact-free

image gathers, at least when the DSR condition holds. The right-hand panel in Figure 11 presents an angle domain image gather following the prescription of (Prucha et al., 1999), which illustrates this contention.

Combining horizontal and vertical offsets: the Traveltime Injectivity Condition

The DSR assumption will not hold, or permit adequate imaging, in complex lithologic environments with substantial lateral and vertical velocity variation, vertical or overhanging reflectors, etc. However, two other conditions, both necessary in general for imaging given correct velocity, are also sufficient to ensure that the energy in a *properly filtered* source-receiver restricted offset image volumes is concentrated (i) at zero offset, and possibly (ii) at offsets greater than a minimum which depends on various characteristics of the velocity through its ray geometry. That is, in absence of the DSR restriction, energy may appear at nonzero offsets, even with correct velocity, but not within a corridor about zero offset, except at zero offset.

This section explains the physical and geometric significance of these conditions, and the necessity of filtering. Mathematical details appear in Appendix C.

The first of these two conditions is the "no scattering over π" condition identified already in (Rakesh, 1988) as essential to accurate migration. That is, no energy along direct rays connecting source to receiver can appear in the data submitted to migration. We quantify this condition by demanding that the scattering angle for all ray pairs involved in image construction be less than a maximum angle, which is less than π. This "maximum scattering angle" or MSA condition can in principle be enforced by ray-tracing and selective muting and Radon filtering.

The second condition is the *Traveltime Injectivity Condition* or TIC (Ten Kroode et al., 1998; Nolan and Symes, 1997). This condition is in general necessary for artifact-free postmigration stacks - i.e. absence of mispositioned reflectors, not in the prestack image volume but in the final stacked image. TIC mandates that *along any pair of rays, at most one point of intersection exists with a given (total) traveltime.* Clearly TIC is also implied by the DSR condition, so TIC generalizes DSR. It is also clear that TIC can be violated - see the cited references for examples.

Under some circumstances standard migration operators (i.e. adjoints of linearized modeling operators) may produce artifact-free images even when TIC is violated - see (Stolk, 2000) for a discussion of this point. However in general TIC is necessary for artifact-free imaging. A quantitative form of TIC, with a specific estimate of distance vs. time along imaging ray pairs, is explained in Appendix C.

It is less clear how TIC may be enforced for the data submitted to migration. The present results, like those of (Ten Kroode et al., 1998), simply presume that (the quantitative form of) TIC holds.

As explained earlier, a simple variable count suggests that unambiguous images can only be accomplished by restricting the offset to planes (or lines, for 2D shot-geophone migration). However, without the DSR hypothesis, it is easy to see that the horizontal

offset imaging operator, $\bar{F}_z$, cannot have the focussing property, i.e. focus energy at zero offset for correct velocity.

Figures 9 and 10 show why this is so. Both figures are meant to cartoon imaging at correct velocity, which for convenience is assumed constant near the image point (hence the locally straight rays). In Figure 9, two rays image an event at their intersection on a reflector with nonzero z component of dip. Note that as one moves away from the image point, keeping the total time along the two rays the same, the difference in z components of the ray locations unavoidably grows, so that these (unrestricted) source-receiver image points do not appear in the horizontal offset operator output. That is, only the zero offset image survives restriction to horizontal offset. On the other hand, Figure 10 shows an image point on a vertical reflector; clearly one can move away from the image point, maintaining the same total time, in such a way that these other unrestricted image points have the same z components hence survive the restriction to horizontal offset. Obviously in this case the output of $\bar{F}_z$ will have energy at all offsets sufficiently close to zero, and the focussing property is lost.

Examples presented in (Biondi and Shan, 2002) demonstrate this "smearing" of image gathers in horizontal offset shot-geophone migration ($\bar{F}_z^*$) as reflector dip approaches horizontal. Here we give a simpler example which exactly corresponds to the cartoon 10. The velocity depicted in Figure 12 increases (linearly) with depth to the right of the vertical reflector, so generates reflections along ray pairs, one of which has turned. Sources and receivers to the right of the reflector record data, of which a typical shot gather is depicted in 13. We have used a slight modification of the frequency-domain two-way migration algorithm proposed by (Pratt et al., 1998). The horizontal offset image gather (Figure 14) at the location of the reflector shows some energy focussed at zero offset but also a great deal of low-frequency energy is spread over the entire offset range - note that according to the color scale, only small positive values but large negative values occur, indicating the presence of large near-DC components. This low-frequency smear is the residue of destructive interference of passband energy imaged and many contiguous image points, as predicted by the argument illustrated in Figure 10.

Figure 9 on the other hand suggests that this reflector should be well-imaged by a *vertical* offset image gather, and this is indeed the case. Figure 15 shows vertical offset image gathers at two depths: the energy is well-focussed at zero (vertical) offset and localized on the reflector.

Note that the absence of nonzero offset image energy suggested by Figure 9 is a *local* phenomenon. That is, the rays may curve in such a way that points may appear with the same total travel time and z coordinates, sufficiently far away from the physical scattering point - Figure 17 cartoons this situation. The time difference cannot be close to zero, however. As shown in Appendix C, together with TIC and MSA this minimum time difference implies that the offset of any image energy at nonzero offset also exceeds a minimum.

The inescapable conclusion is that horizontal offset shot-geophone migration cannot image (near) vertical reflectors without degrading the focussing property characteristic

of correct velocity. Precisely analogous reasoning shows that x- and y-axis vertical offset shot-geophone migration ($\bar{F}_x^*, \bar{F}_y^*$) cannot image dips perpindicular to the x-axis and y-axis respectively without smearing in the restricted offset.

On the other hand, any particular dip is well-imaged by at least one of these operators, with focussing at zero offset at least locally, as argued above in the horizontal offset case. The paper (Biondi and Symes, 2004) presents one method to take advantage of this fact to image all dips, using transformation to the angle domain. An alternative method works through image filtering, as follows.

Define a filter $\bar{\Psi}_z$ which annihilates the plane wave components of horizontal offset reflectivities $\bar{R}_z$ with small k_z (relative to the other plane wave components). A precise definition of such a filter is givien in Appendix D. Then for any horizontal offset reflectivity $\bar{R}_z$, the filtered reflectivity $\bar{\Psi}_z\bar{R}_z$ *does not contain* vertically oriented reflectors, so that the relationship depicted in Figure 10 does not occur, and events in $\bar{F}[v]_z\bar{\Psi}_z\bar{R}_z$ are imaged only at zero offset.

Since the relation between event and reflector image location is the same with modeling and migration, this reasoning indicates that:

The quantitative versions of TIC and MSA, which are necessary for reliable imaging, imply that the filtered horizontal offset migration $R_z = \bar{\Psi}_z\bar{F}_z[v]^*d$ has (for correct migration velocity v) (i) energy at zero offset, and (ii) all other image energy confined to offsets at least $h_{\min}$.

Note the contrast of this statement with the result obtained under the more restrictive DSR assumption: it is possible for the filtered migrated image volume to have energy at nonzero offset, even when the velocity is correct - this was impossible under DSR - but not inside the corridor $h < h_{\min}$.

R_z, computed as specified above, images reflectors with nonhorizontal dips. To fill out the dip range, one can adjoin the similarly computed vertical offset images

$$R_x = \bar{\Psi}_x\bar{F}_x[v]^*d,\ R_y = \bar{\Psi}_y\bar{F}_y[v]^*d$$

The three volumes R_z, R_y, R_z together image all dips, and each has the local focussing property analogous to that already described for $\bar{R}_z$.

As discussed in the section below on implementation, the cost of computing image gathers at sufficiently dense midpoints to support midpoint dip filtering may be prohibitive. Dense midpoint sampling of image gathers is surely unnecessary for velocity analysis in any case. Instead of midpoint dip filtering, simple low-cut filtering of $\bar{R}_j$ in j, $j = x, y, z$, is sufficient to remove the low-frequency smear over offset and restore focussing at zero offset.

In the context of the model of Figure 12, filtering in z should simply remove all energy in the horizontal offset image gather ($\bar{R}_z$) at the vertical reflector. Figure 16 shows that this is indeed the case. The filtered versions of the vertical offset image gathers in Figure 15 on the other hand are barely changed at all. Thus the filtered vertical and horizontal offset image gathers *together* capture all of the energy in the data and focus it at zero offset, given the correct velocity model, as predicted by the theory.

As noted in (Biondi and Symes, 2004), it is not possible to simply average the three volumes $\bar{R}_z, \bar{R}_y, \bar{R}_z$ to form a single image volume, when the velocity is not correct, due to a variation on the familiar phenomenon of image point dispersal. Of course when the velocity is correct, the versions of reflectors contained in the image volumes overlap, and can be added together to form a final image volume. [The filter definition explained in Appendix A is formulated to guarantee that this is possible, with no gaps and no artificially enhanced amplitudes.] However for velocity analysis (i.e. before a correct velocity has been achieved) these three volumes must be maintained as separate. See (Biondi and Symes, 2004) for a proposal to produce a single angle domain image volume which at least in some cases permits averaging the various image volumes (after Radon transform) even with incorrect velocity.

IMPLEMENTATION

The computation of S-G image gathers adds a premium to the computational cost of two way reverse time migration, which is itself costly compared to other migration methods (Yoon et al., 2003). Even a cursory examination of the S-G imaging equation (8) suggests that the additional cost could be considerable, and that the number of midpoints at which image gathers are computed will have to be limited somehow. Since the number of midpoints is related to velocity complexity, and velocity analysis typically uses only a subset of all theoretically possible midpoints, this limitation is not necessarily in itself an impediment. However the midpoint dip filtering operator, on which the theory depended to avoid imaging failure, is no longer available when midpoints are decimated.

This section presents a preliminary assessment of the cost of two-way S-G CIG formation, and suggests a functional alternative to midpoint dip filtering which does not require dense midpoint sampling. We discuss in detail the cost of 2D S-G migration to produce horizontal offset CIG; vertical offset CIGs have a similar cost profile, as do the corresponding 3D computations.

We assume a typical finite-difference simulation approach, with the additional feature that the domain of each simulation is limited by the distance which waves actually travel during the scattering process. Thus the number of points in the x direction which actually figure in an particular shot simulation, say N_x, is proportional to N_t, the number of time steps required, and decoupled from N_s, the number of shots (and from the total length of the survey line). Similar considerations apply to N_z.

The cost of a single shot gather simulation is $S_0 N_x N_z N_t \simeq S_0 C_x C_z N_t^3$, where S_0 is the number of floating point operations per stencil, and C_x, C_z reflects the proportionality between N_x, N_z and N_t. The cost of backpropagating the data is similarly $S_1 N_x N_z N_t \simeq S_1 C_x C_z N_t^3$, in which the stencil count for the adjoint state equation, used in backpropagation, is larger than than for the simulation itself - typically $S_1 \simeq 2S_0$. Computation of the migrated image (at offset zero) costs one additional flop per spacetime gridpoint, and we amalgamate this cost with that of the backpropagation.

The cost of the cross-correlation (equation (8)) to produce an HOCIG at a single midpoint, per shot, is is $N_h N_z N_t$. The range of offsets required in the CIG is a consequence

of its purpose, namely velocity analysis, and is a function of the kinematic correctness of the migration velocity model. For a kinematically correct model, the CIGs are as concentrated as possible at zero offset, and the range of offset in the CIG need be only a Fresnel zone or so. For incorrect models, the CIG must extend in offset far enough that no significant amount of image energy lies outside the CIG. The relation between "goodness" of velocity model and range of offset required to assure a constructive velocity update is not well understood at present. We will capture this (unknown) quantity in a proportionality constant E: $N_h = EN_x = EC_xN_t$. Thus the cost per midpoint per shot of CIG computation is $EC_xC_zN_t^3$.

The number of midpoints computed per shot is proportional to the $x - extent$ of the computational domain $N_x\Delta x$, as the wavefields in equation (8) vanish outside the range of x occuring in the shot gather computation. The ratio, M, is the computed midpoint density per unit length: $N_m = MN_x\Delta x = MN_x\bar{v}\Delta t$, $\bar{v}$ being a typical velocity. Note that we do not presume that N_m scales with N_t, or inversely with $1/\Delta t$, as do the other quantities in this computation: the density of CIGs is related to the required resolution of the velocity model, which should in principle be independent of the frequency content of the data, insofar as the Born approximation is appropriate (i.e. insofar as migration makes sense).

Thus the cost per shot of CIG formation is $N_mN_hN_zN_t = EMC_xC_z\bar{v}\Delta tN_t^4$
$= EM\bar{v}TC_xC_zN_t^3$, with $T = N_t\Delta t$ being the simulation time.

The premium required to produce the CIGs, as opposed to the migrated image, is accordingly

$$\frac{(S_0 + S_1 + EM\bar{v}T)C_xC_zN_t^3}{(S_0 + S_1)C_xC_zN_t^3} = 1 + \frac{EM\bar{v}T}{S_0 + S_1}$$

We can see from this simple calculation that the expense of CIG creation will rise with kinematic error in velocity, with lateral complexity of the velocity model required to reduce this kinematic error, and with the maximum depth probed.

Arguably, the product EM may be roughly constant, within an effective velocity analysis process: denser sampling of the velocity model, control of which requires denser sampling of CIGs in midpoint (larger M), should lead to enhanced accuracy of the velocity model (smaller E). The dependence of this "constant" EM on velocity complexity is a natural topic for further research.

Given the necessity to decimate midpoint sampling in creating CIGs, the technique analyzed in the preceding section and Appendix C, midpoint dip filtering, is not available in practice. Some other method is required to insure that energy focusses at zero offset for correct velocity, at least within a corridor of nonzero width.

Our suggested alternative is based on the observation that the bandlimited nature of seismic data implies that high-pass filtering in z (for horizontal offset CIGs) has the effect of placing a lower bound on k_z/k_m, where k_m is the midpoint wavenumber

$$k_m = \sqrt{(k_{s,x} + k_{r,x})^2 + (k_{s,y} + k_{r,y})^2}.$$

In fact, if k denotes the maximum midpoint/depth wavenumber in the image, then

$$\frac{|k_z|}{k_m} \geq \frac{|k_z|}{k}$$

The (local) spatial bandlimit k is related to the temporal bandwidth $\omega_{\max}$, of course, hence varies with the background velocity v. Conceivably one could employ a space-varying high-pass filter to keep the low-cut in k_z a (more or less) constant fraction of the total image bandwidth. We have elect to simply choose a constant low cut.

Low-cut filtering to remove image artifacts has already been illustrated in the example of Figure 16, discussed in the last section.

CONCLUSION

This paper has provided a novel description of shot-geophone migration, as the adjoint of a shot-geophone modeling operator which extends ordinary Born modeling. From this point of view, the method of computation used to generate the necessary fields - two way reverse time, two way frequency domain, or depth extrapolation - is a secondary detail, and indeed this paper exhibits examples of all three methods. A Kirchhoff-like formulation even exists, though its utility as a computational method may not be great.

Using our characterization of shot-geophone migration and the ray-theoretic analysis of imaging pioneered in (Rakesh, 1988), we have given a simple argument for the very important result of (Stolk and De Hoop, 2001): under the DSR assumption, shot-geophone migration produces a prestack horizontal offset image volume free of kinematic artifacts. That is, assuming DSR and correct velocity, all image energy focusses at zero offset (or, in the angle domain, at zero slope - see (Sava et al., 2001)). This property stands in dramatic contrast to the ubiquitous presence of such artifacts in standard prestack imaging (Stolk and Symes, 2004).

We have also shown how to use non-horizontal offsets to produce multiple image volumes in which the focussing-at-zero-offset property is preserved, even in the presence of turning ray energy, through judicious filtering. Our analysis of this construction suggests that the focussing property may be local when the DSR property is violated: that is, image artifacts may exist at sufficiently large offsets. The extent to which such artifacts may occur, and the implications of their existence for velocity analysis, remain to be investigated.

Some of the early literature on shot-geophone migration suggested its possible use in velocity analysis - see for example (Schultz and Sherwood, 1982). This possibility seems to have been little explored in the interim (a partial exception being focussing analysis as introduced in (Faye and Jeannot, 1986)). The properties of shot-geophone migration explained in this paper suggest that this approach to imaging may be a particularly appropriate tool for velocity analysis in complex structure.

Acknowledgements

This work was supported in part by National Science Foundation, and by the sponsors of The Rice Inversion Project (TRIP).

REFERENCES

Biondi, B. and Shan, G. (2002). Prestack imaging of overturned reflections by reverse time migration. In *Expanded Abstracts, Society of Exploration Geophysicists, 72nd Annual International Meeting*, pages 1284–1287, Tulsa. SEG.

Biondi, B. and Symes, W. (2004). Angle-domain common-image gathers for migration velocity analysis by wavefield-continuation imaging. *Geophysics*, (in press).

Claerbout, J. (1985). *Imaging the Earth's Interior*. Blackwell Scientific Publishers, Oxford.

Duistermaat, J. (1973). Fourier integral operators. Lecture notes, Courant Institute, New York.

Faye, J.-P. and Jeannot, J.-P. (1986). Prestack migration velocities from focusing depth analysis. In *Expanded Abstracts, Society of Exploration Geophysicists, 56th Annual International Meeting*, pages 438–440, Tulsa. SEG.

Hormander, L. (1983). *The Analysis of Linear Partial Differential Operators*, volume I. Springer Verlag, Berlin.

Kleyn, A. (1983). *Seismic Reflection Interpretation*. Applied Science Publishers, New York.

Lailly, P. (1983). The seismic inverse problem as a sequence of before-stack migrations. In Bednar, J. et al., editors, *Conference on Inverse Scattering: Theory and Applications*, pages 206–220. SIAM, Philadelphia.

Nolan, C. and Symes, W. (1997). Global solution of a linearized inverse problem for the wave equation. *Comm. P. D. E.*, 22:919–952.

Nolan, C. J. and Symes, W. W. (1996). Imaging and conherency in complex structure. In *Expanded Abstracts, Society of Exploration Geophysicists, 66th Annual International Meeting*, pages 359–363, Tulsa. SEG.

Pratt, R. G., Shin, C., and Hicks, G. J. (1998). Gauss-newton and full newton methods in frequency-space seismic waveform inversion. *Geophys. J. Int.*, 133:341–362.

Prucha, M., Biondi, B., and Symes, W. (1999). Angle-domain common image gathers by wave-equation migration. In *Expanded Abstracts,Society of Exploration Geophysicists, 69th Annual International Meeting*, pages 824–827. SEG.

Rakesh (1988). A linearized inverse problem for the wave equation. *Comm. on P.D.E.*, 13(5):573–601.

Rickett, J. and Sava, P. (2002). Offset and agnle-domain common image-point gathers for shot profile migration. *Geophysics*, 67:883–889.

Sava, P., Biondi, B., and Fomel, S. (2001). Amplitude preserved common image gathers by wave equation migration. In *Expanded Abstracts, Society of Exploration Geophysicists, 71st Annual International Meeting*, pages 296–299, Tulsa. SEG.

Sava, P. and Fomel, S. (2003). Angle-domain common-image gathers by wavefield continuation methods. *Geophysics*, 68:1065–1074.

Schultz, P. and Sherwood, J. (1982). Depth migration before stack. *Geophysics*, 45:376–393.

Stolk, C. (2000). *On the modeling and inversion of seismic data*. PhD thesis, Universiteit Utrecht.

Stolk, C. C. (2002). Microlocal analysis of the scattering angle transform. *Comm. P. D. E.*, 27:1879–1900.

Stolk, C. C. and De Hoop, M. V. (2001). Seismic inverse scattering in the 'wave-equation' approach. Preprint 2001-047, The Mathematical Sciences Research Institute, http://msri.org/publications/preprints/2001.html.

Stolk, C. C. and Symes, W. W. (2004). Kinematic artifacts in prestack depth migration. *Geophysics*, 69:562–575.

Tarantola, A. (1987). *Inverse Problem Theory*. Elsevier.

Taylor, M. (1981). *Pseudodifferential Operators*. Princeton University Press, Princeton, New Jersey.

Ten Kroode, A. P. E., Smit, D. J., and Verdel, A. R. (1998). A microlocal analysis of migration. *Wave Motion*, 28:149–172.

Whitmore, N. D. (1983). Iterative depth migration by backwards time propagation. In *Expanded Abstracts,Society of Exploration Geophysicists, 53rd Annual International Meeting*, page S10.1. SEG.

Xu, S., Chauris, H., Lambaré, G., and Noble, M. (2001). Common angle migration: A strategy for imaging complex media. *Geophysics*, 66(6):1877–1894.

Yilmaz, O. (1987). Seismic data processing. In *Investigations in Geophysics No. 2*. Society of Exploration Geophysicists, Tulsa.

Yoon, K., Shin, C., Suh, S., Lines, L., and Hong, S. (2003). 3d reverse-time migration using hte acoustic wave equation: An experience with the SEG/EAGE data set. *The Leading Edge*, 22:38.

APPENDIX A

This appendix gives a quick derivation of equation (8). For several examples of this type of computation, see (Tarantola, 1987)

The claim is that

$$F[v]^* d(\mathbf{x}, \mathbf{h}) = \int dx_s \int_0^T dt\, q(\mathbf{x}+\mathbf{h}, t; \mathbf{x}_s) \frac{\partial^2 G}{\partial t^2}(\mathbf{x}-\mathbf{h}, t; \mathbf{x}_s)$$

where *adjoint field* q satisfies $q \equiv 0$, $t \geq T$ and

$$\left(\frac{1}{v^2}\frac{\partial^2}{\partial t^2} - \nabla^2\right) q(\mathbf{x}, t; \mathbf{x}_s) = \int dx_r \, d(\mathbf{x}_r, t; \mathbf{x}_s)\delta(\mathbf{x} - \mathbf{x}_r)$$

and G is the reference Green's function.

To see this, form the standard inner products in the appropriate spaces (image on the left, data on the right), and recall that $\bar{F}[v]R(\mathbf{x}_r, t; \mathbf{x}_s) = u(\mathbf{x}_r, t; \mathbf{x}_s)$, where $u(\mathbf{x}, t; \mathbf{x}_s)$ satisfies

$$\left(\frac{1}{v^2(\mathbf{x})}\frac{\partial^2}{\partial t^2} - \nabla^2\right) u(\mathbf{x}, t; \mathbf{x}_s) = \int dh \, R(\mathbf{x} - \mathbf{h}, \mathbf{h})\frac{\partial^2 G}{\partial t^2}(\mathbf{x} - 2\mathbf{h}, t; \mathbf{x}_s)$$

So

$$< \bar{F}[v]^* d, R > = < d, \bar{F}[v]R >$$

$$= \int\int dx_s \, dx_r \int_0^T dt \, d(\mathbf{x}_r, t; \mathbf{x}_s) u(\mathbf{x}_r, t; \mathbf{x}_s)$$

$$= \int dx_s \int dx \int_0^T dt \left\{ \int dx_r \, d(\mathbf{x}_r, t; \mathbf{x}_s)\delta(\mathbf{x} - \mathbf{x}_r) \right\} u(\mathbf{x}, t; \mathbf{x}_s)$$

$$= \int dx_s \int dx \int_0^T dt \left[\left(\frac{1}{v^2}\frac{\partial^2}{\partial t^2} - \nabla^2\right) q \right] u(\mathbf{x}, t; \mathbf{x}_s)$$

$$= \int dx_s \int dx \int_0^T dt \left[\left(\frac{1}{v^2}\frac{\partial^2}{\partial t^2} - \nabla^2\right) u \right] q(\mathbf{x}, t; \mathbf{x}_s)$$

(boundary terms in integration by parts vanish because (i) $u \equiv 0$, $t << 0$; (ii) $q \equiv 0$, $t >> 0$; (iii) both vanish for large $\mathbf{x}$, at each t)

$$= \int dx_s \int dx \int_0^T dt \int dh \, R(\mathbf{x} - \mathbf{h}, \mathbf{h})\frac{\partial^2 G}{\partial t^2}(\mathbf{x} - 2\mathbf{h}, t; \mathbf{x}_s) q(\mathbf{x}, t; \mathbf{x}_s)$$

$$= \int dx_s \int dx \int_0^T dt \int dh \, R(\mathbf{x}, \mathbf{h})\frac{\partial^2 G}{\partial t^2}(\mathbf{x} - \mathbf{h}, t; \mathbf{x}_s) q(\mathbf{x} + \mathbf{h}, t; \mathbf{x}_s)$$

$$= < R, \bar{F}[v]^* d >$$

from which you can immediately read off $\bar{F}[v]^*$, which has the form claimed. **q.e.d.**

APPENDIX B

In this appendix we establish the relation between the appearance of events in the data and the presence of reflectors in the migrated image. This relation is the *same* for the forward modeling operator and for its adjoint, the migration operator.

The reasoning presented here shares with (Stolk and De Hoop, 2001) the identification of events, respectively reflectors, by high frequency asymptotics in phase space, but differs

in that it does not explicitly use the oscillatory integral representation of $F[v]$ derived in the last section. Instead, this argument follows the pattern of Rakesh's analysis of shot profile migration kinematics (Rakesh, 1988). It can be made mathematically rigorous, by means of the so-called Gabor calculus in the harmonic analysis of singularities (see (Duistermaat, 1973) Ch. 1).

The appearance of an event at a point $(\mathbf{x}_s, \mathbf{x}_r, t_{sr})$ in the data volume is equivalent to the presence of a sizeable Fourier coefficient for a plane wave component

$$e^{i\omega(t-\mathbf{p}_s\cdot\mathbf{y}_s-\mathbf{p}_r\cdot\mathbf{y}_r)}$$

in the acoustic field for frequencies ω within the bandwidth of the data, even after muting out all events at a small distance from $(\mathbf{x}_s, \mathbf{x}_r, t_{sr})$.

Note that the data does not necessarily fully determine this plane wave component, i.e. the full 3D event slownesses $\mathbf{p}_s, \mathbf{p}_r$. In this appendix, $\mathbf{p}_s, \mathbf{p}_r$ are assumed to be compatible with the data, in the sense just explained.

Assume that these frequencies are high enough relative to the length scales in the velocity that such local plane wave components propagate according to geometric acoustics. This assumption tacitly underlies much of reflection processing, and in particular is vital to the success of migration.

That is, solutions of wave equations such as (11) carry energy in local plane wave components along rays. Let $(\mathbf{X}_r(t), \mathbf{P}_r(t))$ denote such a ray, so that $\mathbf{X}_r(t_{sr}) = \mathbf{x}_r, \mathbf{P}_r(t_{sr}) = \mathbf{p}_r$. Then at some point the ray must pass through a point in phase space at which the source term (right hand side) of equation (11) has significant energy - otherwise the ray would never pick up any energy at all, and there would be no event at time t_{sr}, receiver position $\mathbf{x}_r$, and receiver slowness $\mathbf{p}_r$. [Supplemented with proper mathematical boilerplate, this statement is the celebrated *Propagation of Singularities* theorem of Hörmander, (Hormander, 1983; Taylor, 1981).]

The source term involves (i) a product, and (ii) an integral in some of the variables. The Green's function $G(\mathbf{y}_s, t, \mathbf{x}_s)$ has high frequency components along rays from the source, i.e. at points of the form $(\mathbf{X}_s(t_s), \mathbf{P}_s(t_s))$ where $\mathbf{X}_s(0) = \mathbf{x}_s$ and $t_s \geq 0$. [Of course this is just another instance of Propagation of Singularities, as the source term in the wave equation for $G(\mathbf{y}_s, t_s, \mathbf{x}_s)$ is singular only at $(\mathbf{x}_s, 0)$.] That is, viewed as a function of $\mathbf{y}_s$ and t_s, $G(\cdot, \cdot; \mathbf{x}_s)$ will have significant Fourier coefficients for plane waves

$$e^{i\omega(\mathbf{P}_s(t_s)\cdot\mathbf{y}_s+t_s)}$$

We characterize *reflectors* in the same way: that is, there is a (double) reflector at $(\mathbf{y}_s, \mathbf{y}_r)$ if $\bar{R}$ has significant Fourier coefficients of a plane wave

$$e^{i(\mathbf{k}_s\cdot\mathbf{y}'_s+\mathbf{k}_r\cdot\mathbf{y}'_r)}$$

for some pair of wavenumbers $\mathbf{k}_s, \mathbf{k}_r$, and for generic points $(\mathbf{y}'_s, \mathbf{y}'_r)$ near $(\mathbf{y}_s, \mathbf{y}_r)$. Presumably then the product $R(\mathbf{y}'_s, \mathbf{x})G(\mathbf{y}'_s, t_s; \mathbf{x}_s)$ has a significant coefficient of the plane wave component

$$e^{i((\mathbf{k}_s+\omega\mathbf{P}_s(t_s))\cdot\mathbf{y}'_s+\mathbf{k}_r\cdot\mathbf{x}+\omega t_s)}$$

for $\mathbf{y}'_s$ near $\mathbf{y}_s$, $\mathbf{x}$ near $\mathbf{y}_r$; note that implicitly we have assumed that $\mathbf{y}_s$ (the argument of G) is located on a ray from the source with time t_s. The right-hand side of equation (11) integrates this product over $\mathbf{y}_s$. This integral will be negligible unless the phase in $\mathbf{y}_s$ is stationary: that is, to produce a substantial contribution to the RHS of equation (11), it is necessary that

$$\mathbf{y}_s = \mathbf{X}_s(t_s),\ \mathbf{k}_s + \omega \mathbf{P}_s(t_s) = 0 \tag{20}$$

Supposing that this is so, the remaining exponential suggests that the RHS of equation (11) has a sizeable passband component of the form

$$e^{i(\mathbf{k}_r \cdot \mathbf{x} + \omega t_s)}$$

for $\mathbf{x}$ near $\mathbf{y}_r$. As was argued above, this RHS will give rise to a significant plane wave component in the solution u arriving at $\mathbf{x}_r$ at time $t_{sr} = t_s + t_r$ exactly when a ray arriving at $\mathbf{x}_r$ at time t_{sr} starts from a position in space-time with the location and wavenumber of this plane wave, at time $t_s = t_{sr} - t_r$: that is,

$$\mathbf{X}_r(t_s) = \mathbf{y}_r,\ \omega \mathbf{P}_r(t_s) = \mathbf{k}_r \tag{21}$$

We end this appendix with a remark about the case of *complete coverage*, i.e. sources and receivers densely sample a fully 2D area on or near the surface. Assuming that the effect of the free surface has been removed, so that all events may be viewed as samplings of an upcoming wavefield, the data (2D) event slowness uniquely determines the wavefield (3D) slowness through the eikonal equation. Thus an event in the data is characterized by its (3D) moveout: locally, by a moveout equation $t = T(\mathbf{x}_s, \mathbf{x}_r)$, and infinitesimally by the source and receiver slownesses

$$\mathbf{p}_s = \nabla_{\mathbf{x}_s} T,\ \mathbf{p}_r = \nabla_{\mathbf{x}_r} T$$

In this case, the data event uniquely determines the source and receiver rays.

APPENDIX C

This appendix gives the mathematical details leading to the conclusion:

energy in a properly filtered shot-geophone image volume is concentrated (i) at zero offset, and possibly (ii) at offsets greater than a minimum which depends on various characteristics of the velocity.

This conclusion depends on quantitative expressions of two conditions which are necessary for reliable imaging, as discussed in the section "Combining horizontal and vertical offsets". The first of these is a quantitative version of the "maximum scattering angle", or MSA, condition. This hypothesis was shown to be essential for imaging already in (Rakesh, 1988).

For any pair of rays $(\mathbf{X}_s, \mathbf{P}_s), (\mathbf{X}_r, \mathbf{P}_r)$, the definition of the scattering angle θ is

$$\|v(\mathbf{X}_s)\mathbf{P}_s - v(\mathbf{X}_r)\mathbf{P}_r\|^2 = 2(1 + \cos\theta)$$

The quantitative MSA condition states that there is an angle $\theta_{\max} < \pi$ which is not exceeded by any ray pair carrying significant energy.

At a physical scattering point $\mathbf{x}$, where the rays meet, this means that

$$\|\mathbf{P}_s - \mathbf{P}_r\|^2 \geq 2(1 + \cos\theta_{\max})v^{-2}(\mathbf{x})$$

The second condition is a quantitative version of the Traveltime Injectivity Condition, or TIC, which was shown to be necessary in general for artifact-free imaging in (Ten Kroode et al., 1998). We assume that a constant $K > 0$ exists so that for any two rays $\mathbf{X}_s, \mathbf{X}_r$ meeting at time t_s,

$$\|\mathbf{X}_s(t_s + \tau) - \mathbf{X}_r(t_s + \tau)\| \geq K\frac{|\tau|}{\sqrt{1 + \tau^2}} \tag{22}$$

That is, for small τ, points on the two rays at times $t_s + \tau$ are moving away from each other at rate K, and for large τ are asymptotically at least K apart.

In general, if source and receiver rays $(\mathbf{X}_s, \mathbf{P}_s)$, $(\mathbf{X}_r, \mathbf{P}_r)$ produce an image point for $\bar{F}_z$ (i.e. with $\mathbf{X}_{s,z}(t_s) = \mathbf{X}_{r,z}(t_s)$ then we inherit a trajectory of imaging points for the unrestricted shot-geophone migration operator

$$\tau \to (\mathbf{X}_s(t_s + \tau), \mathbf{X}_r(t_s + \tau))$$

One of these is an image point for $\bar{F}_z$ if $\mathbf{X}_{s,z}(t_s+\tau) = \mathbf{X}_{r,z}(t_s-\tau)$. From the ray equations,

$$\frac{d}{d\tau}[\mathbf{X}_{s,z}(t_s + \tau) - \mathbf{X}_{r,z}(t_s + \tau)] = v^2(\mathbf{X}_s(t_s + \tau))\mathbf{P}_{s,z}(t_s + \tau) - v^2(\mathbf{X}_r(t_s + \tau))\mathbf{P}_{s,z}(t_s + \tau)$$

Suppose that the velocity is correct, so that the rays image at zero offset: $\mathbf{X}_s(t_s) = \mathbf{X}_r(t_s) = \mathbf{x}$. Then

$$\frac{d}{d\tau}[\mathbf{X}_{s,z}(t_s + \tau) - \mathbf{X}_{r,z}(t_s + \tau)]_{\tau=0} = v^2(\mathbf{x})\frac{k_z}{\omega}$$

From the slowness part of the ray equations, it follows that

$$\left\| \frac{d}{d\tau} v^{-2}(\mathbf{X}_a(t_s + \tau))\frac{d}{d\tau}[\mathbf{X}_a(t_s + \tau)] \right\| \leq L,$$

in which a is either s or r and L is a global bound for $\|\nabla \log v\|$. From this is is easy to deduce that another global constant $M > 0$ exists, depending on L and on the max and min values of v, so that

$$\left| \frac{d^2}{d\tau^2}[\mathbf{X}_{s,z}(t_s + \tau) - \mathbf{X}_{r,z}(t_s + \tau)] \right| \leq M$$

for all τ. Thus the smallest nonzero value of τ for which

$$\mathbf{X}_{s,z}(t_s + \tau) - \mathbf{X}_{r,z}(t_s + \tau) = 0$$

has size proportional to k_z:

$$|\tau| \geq \frac{2}{M} v^2(\mathbf{x}) \left| \frac{k_z}{\omega} \right| \tag{23}$$

The foregoing suggests that as $k_z \to 0$, i.e. as reflector dip approaches vertical, then other points with arbitrarily small timeshift may image under application of $\bar{F}_z$, and indeed this is the case. Even worse from the point of view of velocity analysis, focussing at $h_x, h_y = 0$ is lost: according to quantitative TIC (equation (22)), one would expect that the imaging offset would vanish along with the time perturbation τ.

For a horizontal offset reflectivity of the form $R_z(x_s, y_s, x_r, y_r, z)$, define E_z to be the operator, already introduced, which produces a source-receiver reflectivity function:

$$E_z R_z(\mathbf{y}_s, \mathbf{y}_r) = r\left(x_s, y_s, x_r, y_r, \frac{z_s + z_r}{2}\right) \delta(z_s - z_r)$$

Define E_x and E_y similarly. If R is a physical reflectivity, i.e. $R(\mathbf{y}_s, \mathbf{y}_r) = r((\mathbf{y}_s + \mathbf{y}_r)/2)\delta(\mathbf{y}_s - \mathbf{y}_r)$, then there are restricted offset reflectivities R_x, R_y, and R_z for which $R = E_x R_x = E_y R_y = E_z R_z$, eg. $R_x(x, y_s, z_s, y_r, z_r) = r(x, (y_s + y_r)/2, (z_s + z_r)/2)\delta(y_s - y_r)\delta(z_s - z_r)$. That is, a physical reflectivity can be represented as the output of any of the three operators E_x, E_y, E_z.

Pick a number $\alpha > 1$. In Appendix D we show how to construct a triple of spatial filter operators Ψ_x, Ψ_y, Ψ_z so that

- $$\Psi_x(\mathbf{k}_s, \mathbf{k}_r) + \Psi_y(\mathbf{k}_s, \mathbf{k}_r) + \Psi_z(\mathbf{k}_s, \mathbf{k}_r) \equiv 1$$

  for all $(\mathbf{k}_s, \mathbf{k}_r)$;

- $$\Psi_x(\mathbf{k}_s, \mathbf{k}_r) = 0 \text{ if } |k_{s,x} + k_{r,x}| < \alpha^{-1}\sqrt{|k_{s,x} + k_{r,x}|^2 + |k_{s,z} + k_{r,z}|^2}$$
  $$\Psi_x(\mathbf{k}_s, \mathbf{k}_r) = 1 \text{ if } |k_{s,x} + k_{r,x}| > \alpha\sqrt{|k_{s,x} + k_{r,x}|^2 + |k_{s,z} + k_{r,z}|^2}$$

  and similarly for Ψ_y, Ψ_z.

If the reflector wavenumber $(\mathbf{k}_s, \mathbf{k}_r)$ is such that $\Psi_z(\mathbf{k}_s, \mathbf{k}_r) > 0$, then from the defining properties of Ψ_z it follows that

$$(1 + \alpha^2)\frac{|k_{s,z} + k_{r,z}|^2}{\omega^2} \geq \frac{\|\mathbf{k}_s + \mathbf{k}_r\|^2}{\omega^2} = \|\mathbf{P}_s - \mathbf{P}_r\|^2$$
$$\geq 2(1 + \cos\theta_{\max})v^{-2}(\mathbf{x}) \tag{24}$$

Introduce filters $\bar{\Psi}_x$, $\bar{\Psi}_y$, and $\bar{\Psi}_z$ on restricted offset reflectivities, defined by the relation

$$\Psi_x E_x = E_x \bar{\Psi}_x \tag{25}$$

and similarly for $\bar\Psi_y$ and $\bar\Psi_z$. These filters have the properties

$$\bar\Psi_z(k_{s,x},k_{s,y},k_{r,x},k_{r,y},k_z)=0 \text{ if } |k_z|<\alpha^{-1}\sqrt{|k_{s,x}+k_{r,x}|^2+|k_{s,y}+k_{r,y}|^2}$$

$$\bar\Psi_z(k_{s,x},k_{s,y},k_{r,x},k_{r,y},k_z)=1 \text{ if } |k_z|>\alpha\sqrt{|k_{s,x}+k_{r,x}|^2+|k_{s,y}+k_{r,y}|^2}$$

and similarly for $\bar\Psi_x,\bar\Psi_y$.

Now suppose that horizontal offset reflectivity R_z contains a physical reflectivity

$$R_z(x_s,y_s,x_r,y_r,z)=r(x,y,z)\delta\left(x-\frac{x_s+x_r}{2}\right)\delta\left(y-\frac{y_s+y_r}{2}\right)+...$$

and that there is a significant component with of the physical reflectivity with vertical wavenumber k_z *after filtering by* $\bar\Psi_z$. THat is, for rays $(\mathbf{X}_s,\mathbf{P}_s),(\mathbf{X}_r,\mathbf{P}_r)$ and scattering time t_s, the rays intersect at $\mathbf{x}$ with the scatterer wavenumber $\omega(\mathbf{P}_r(t_s)-\mathbf{P}_s(t_s))$ having z component k_z. From relations (25, 24) it follows that

$$\frac{k_z^2}{\omega^2}\geq\frac{2(1+\cos\theta_{\max})}{(1+\alpha^2)}v^2(\mathbf{x}) \tag{26}$$

From inequalities (26, 23), it follows that any other point on these two rays which are imaged in $\bar\Psi_z R_z$, i.e. at which $\mathbf{X}_{s,z}(t_s+\tau)=\mathbf{X}_{r,z}(t_s+\tau)$ for some τ, requires that

$$|\tau|\geq\frac{2v(\mathbf{x})}{M}\sqrt{\frac{2(1+\cos\theta_{\max})}{(1+\alpha^2)}} \tag{27}$$

The relations (27, 22) therefore imply that any such secondary image point must occur at an offset $(h_x,h_y)=(\mathbf{X}_{s,x}(t_s+\tau)-\mathbf{X}_{r,x}(t_s+\tau),\mathbf{X}_{s,y}(t_s+\tau)-\mathbf{X}_{y,x}(t_s+\tau))$ satisfying

$$h^2\equiv h_x^2+h_y^2\geq h_{\min}^2 \tag{28}$$

in which $h_{\min}$ depends on max and min values of velocity and velocity gradient length, $\theta_{\max}$, the TIC constant K, and the filter aperture α.

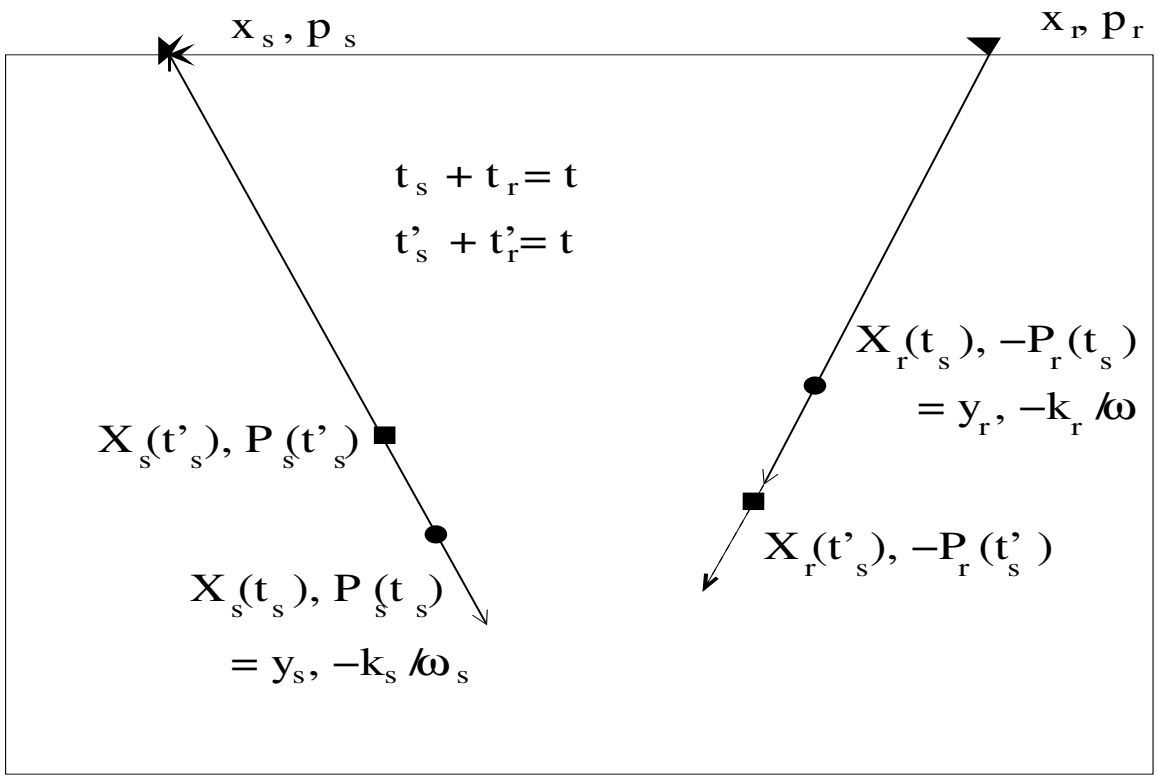

FIG. 1. Ray theoretic relation between data event and double reflector.

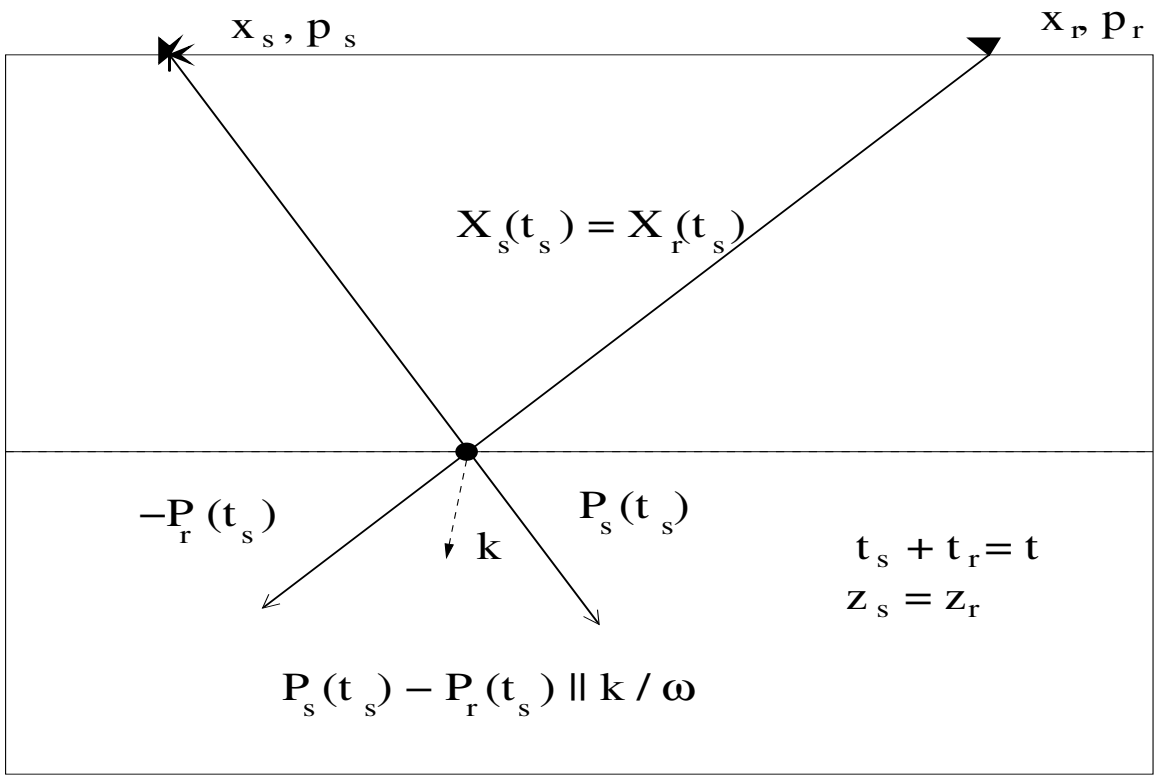

FIG. 2. Ray theoretic relation between data event and physical (single) reflector.

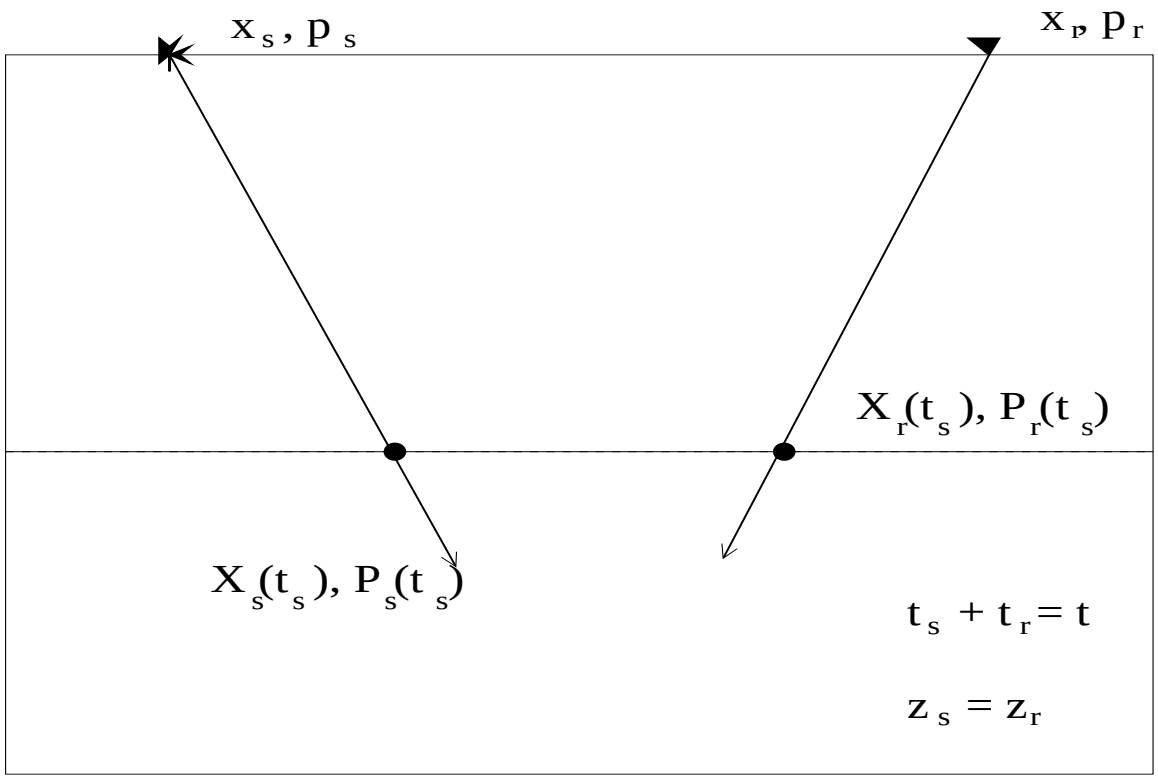

FIG. 3. Ray geometry for double reflector with horizontal offset only

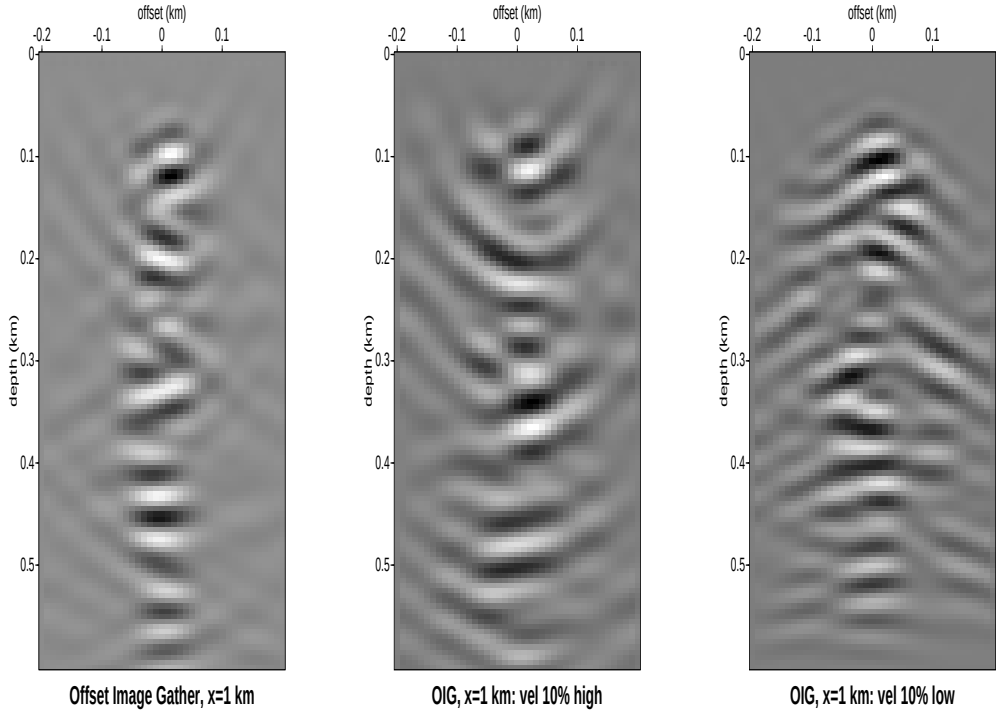

,

,

FIG. 4. Image gathers of data from random reflectivity, from left to right: correct velocity, 10% high, 10% low

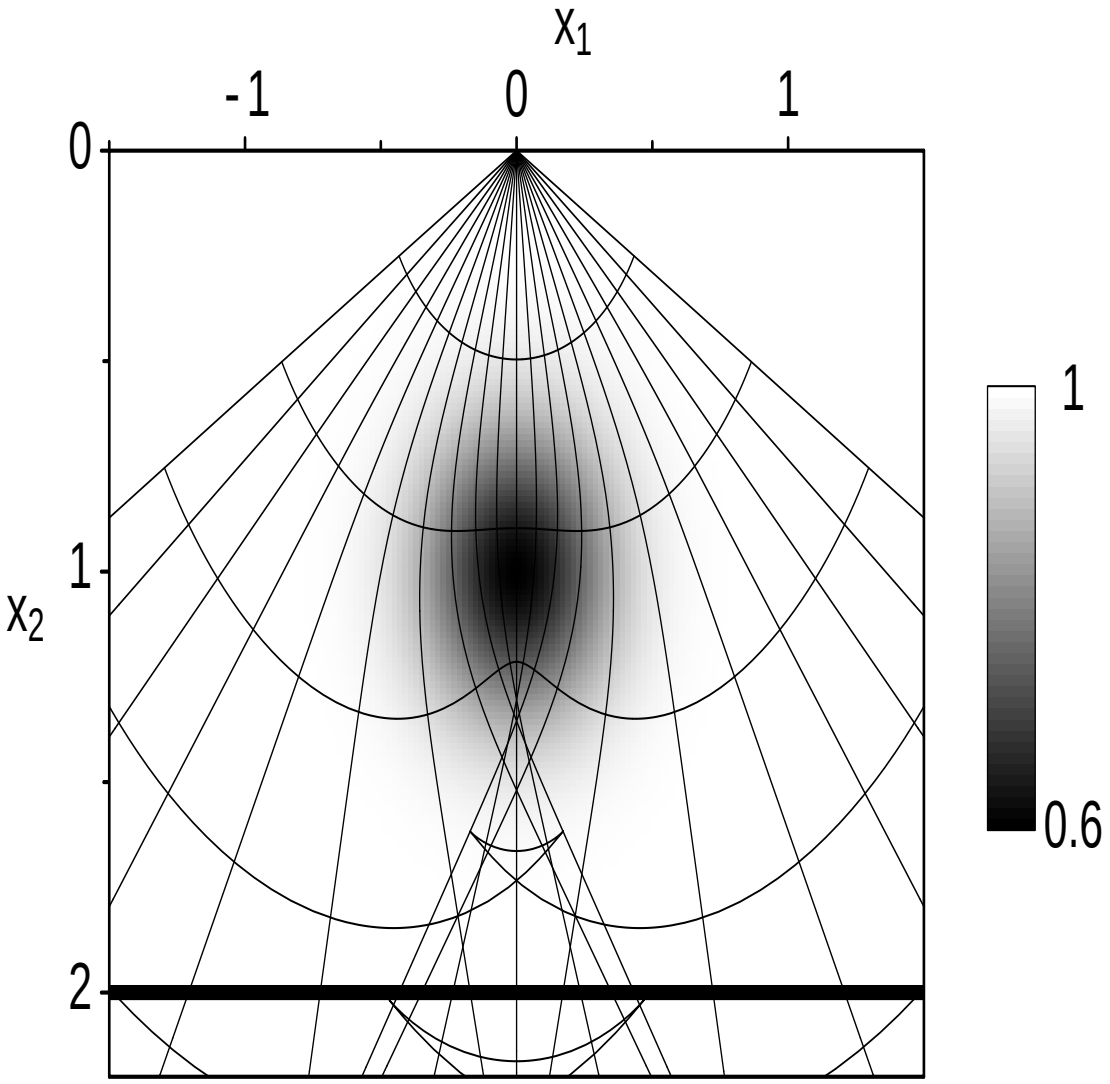

FIG. 5. Lens velocity model, reflector, and modest-offset rays.

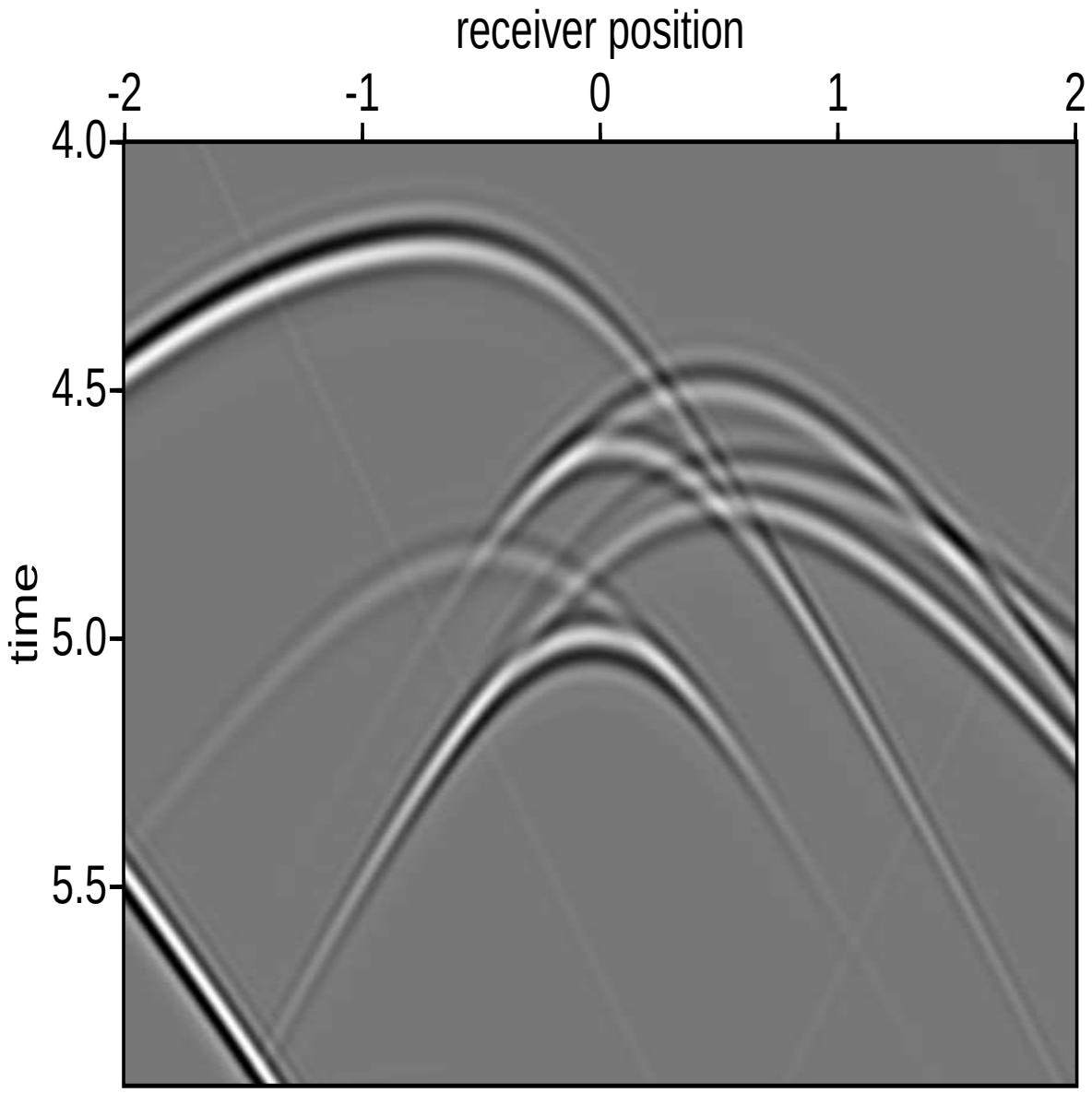

FIG. 6. Lens model: shot record, offset -.5 km

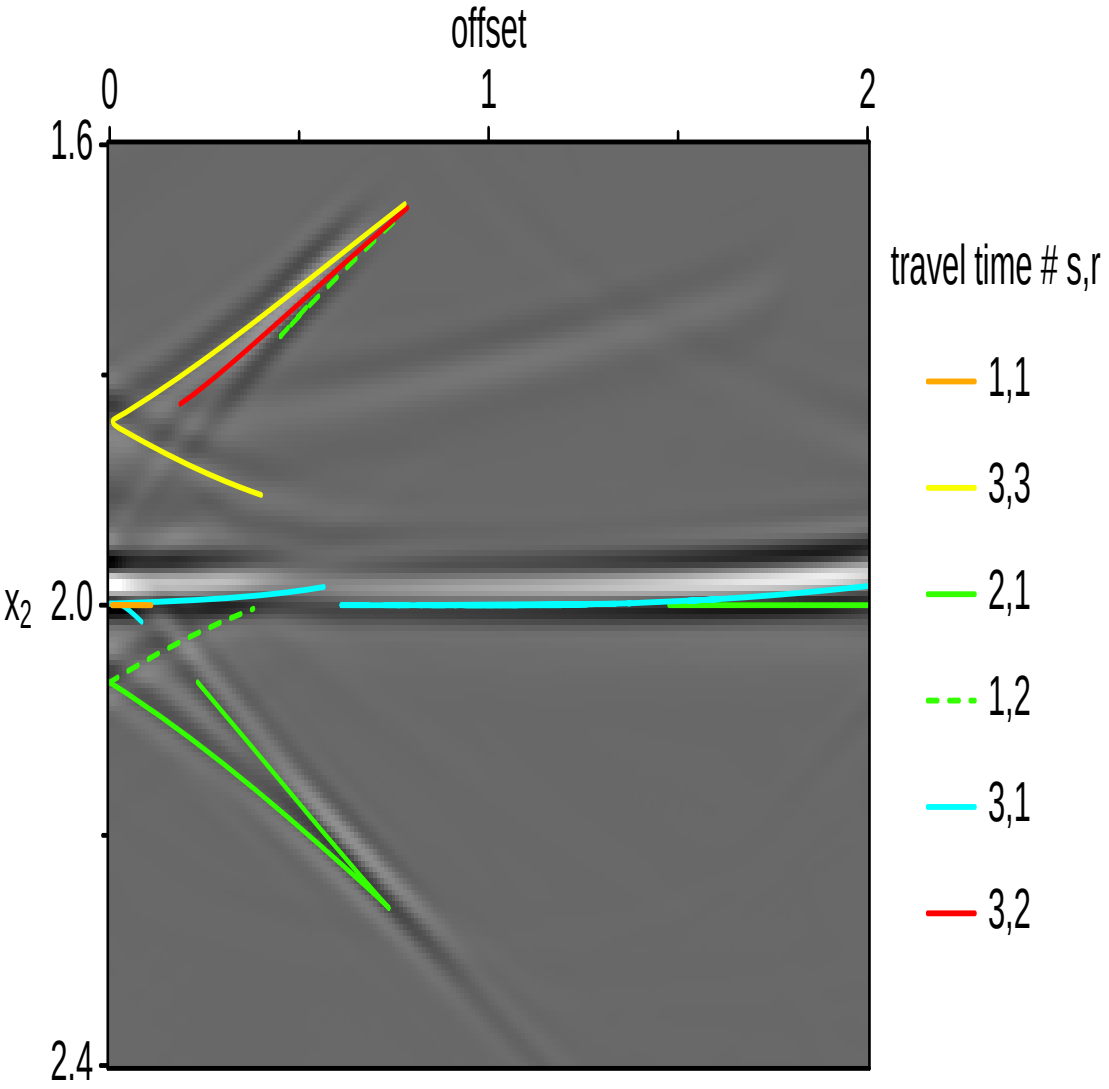

FIG. 7. Lens model: Kirchhoff common offset image gather, $x = 0.3$ km.

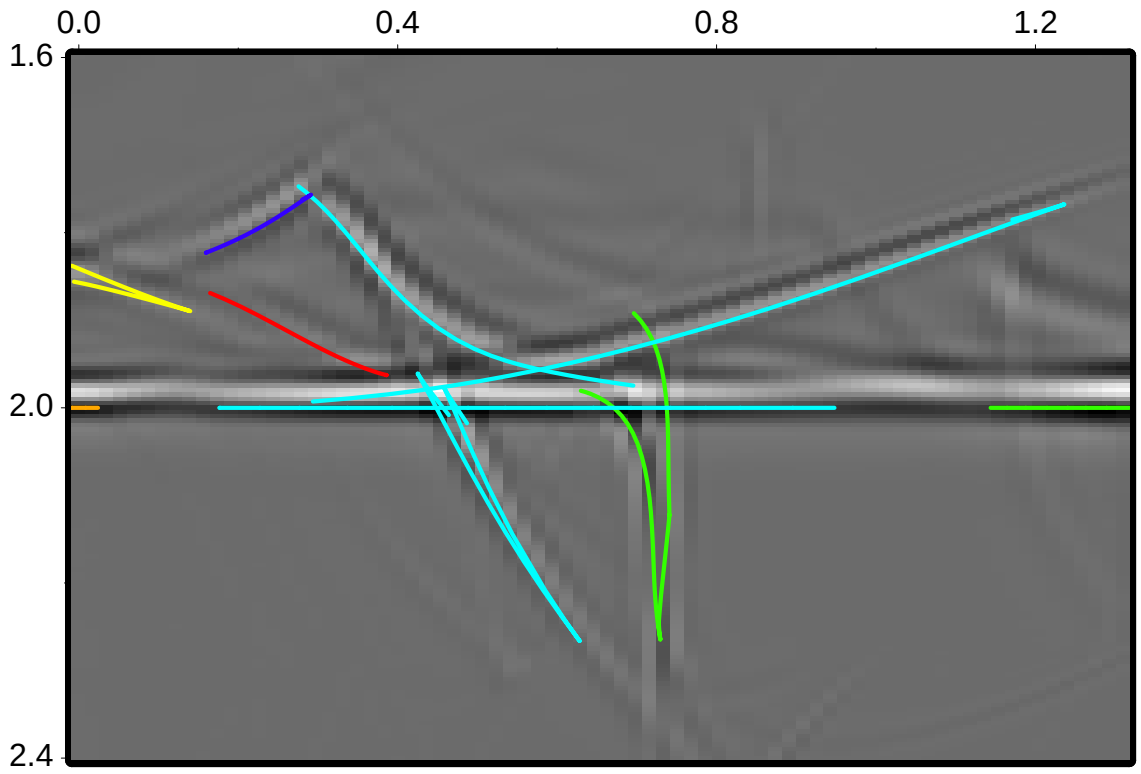

FIG. 8. Lens model: Kirchhoff common scattering angle image gather, $x = 0.3$ km.

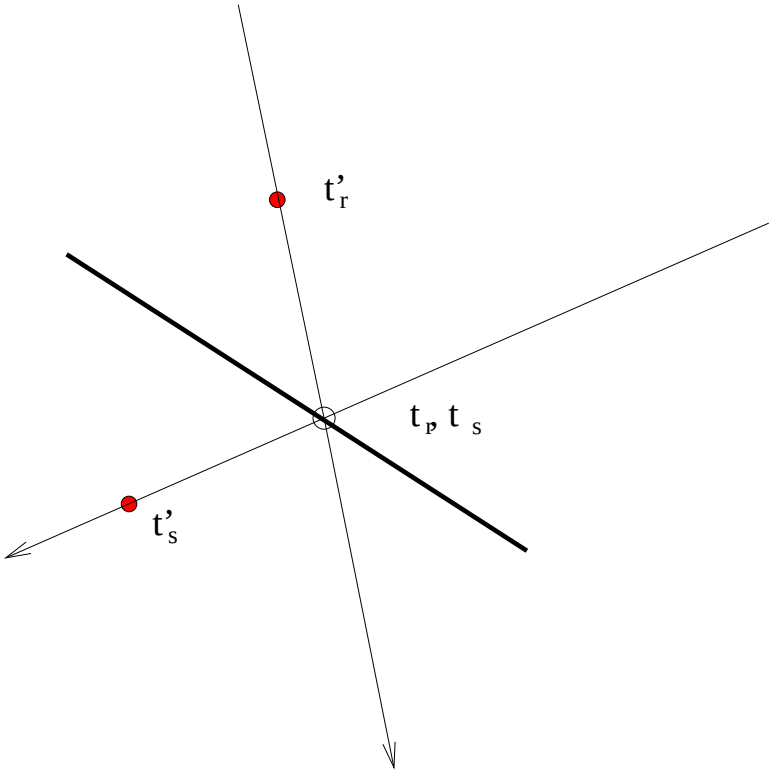

FIG. 9. For a non-vertical reflector (non-horizontal dip), equal time points on incident and reflected rays must have z coordinates differing by an amount proportional to the time difference, at least for times near the reflection time. Therefore horizontal offset image gathers with exhibit focussing only at zero offset or at offsets considerably greater than zero.

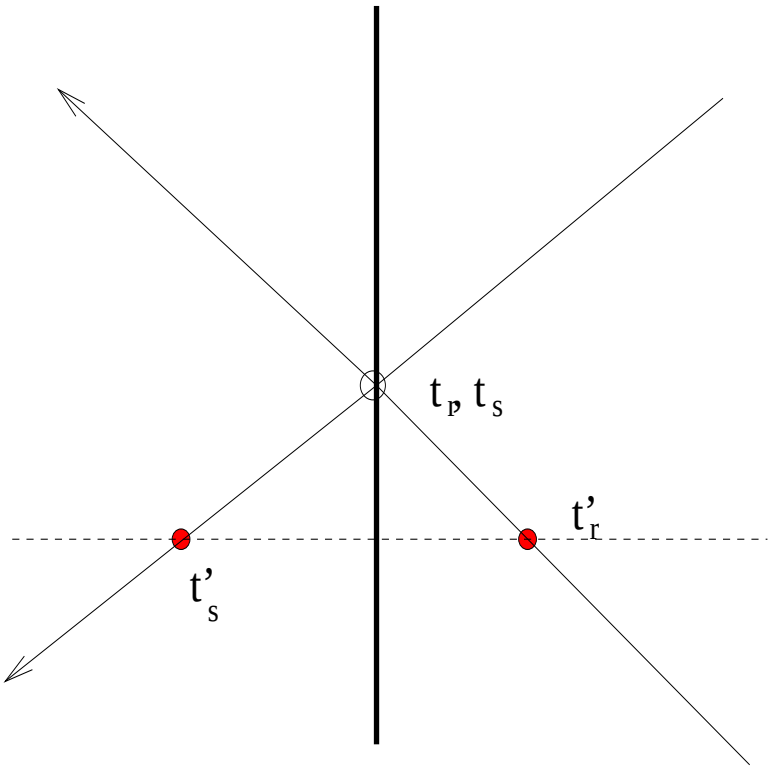

FIG. 10. Incident and reflected rays on a vertical reflector (horizontal dip) may have a sequence of equal time points near the reflection time at which the z coordinates of the rays remain the same - therefore the horizontal offset image gather will contain energy at a range of offsets including zero.

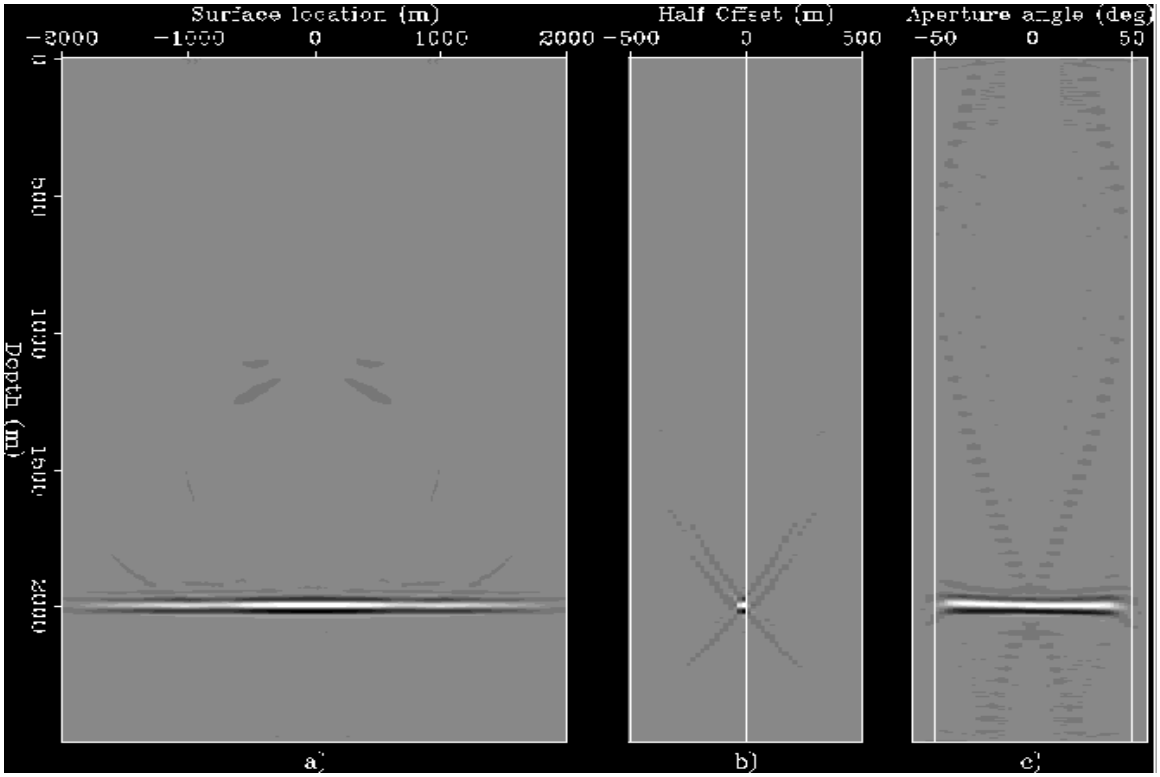

FIG. 11. Left: image of the reflector in the model of Figure 5, obtained by prestack migration of the lens data (Figure 6 shows one of 401 shot gathers), using a depth extrapolation algorithm (Prucha et al., 1999). Center: horizontal offset image gather extracted from the volume, midpoint = center of lens. Right: scattering angle CIG for same data, computed as described in (Prucha et al., 1999).

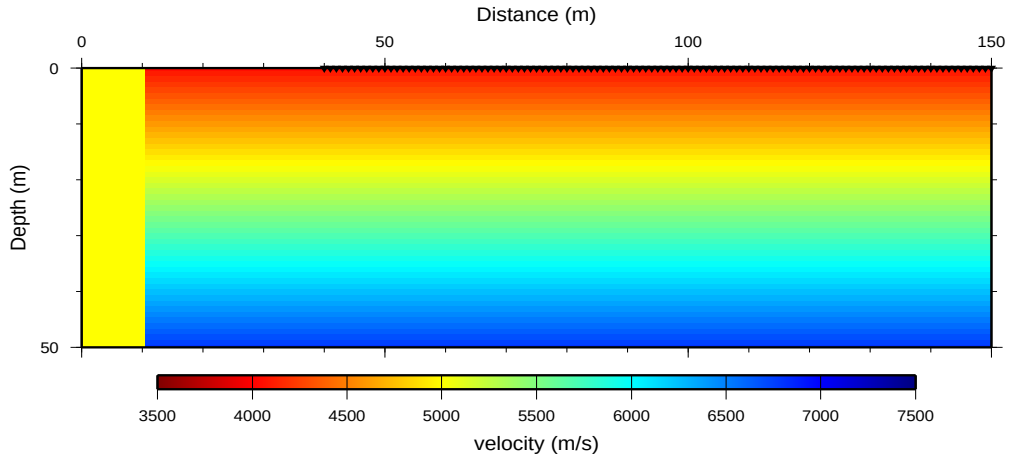

FIG. 12. Acoustic model with linearly increasing velocity and vertical reflector near left edge. Note that dimensions of this model, and frequency ranges of the synthetics obtained from it, are appropriate for near-surface seismology rather than for petroleum exploration. The acquisition geometry is indicated along the top of the figure: 111 source and receiver positions occupy horizontal offsets from 40 m to 150 m, at 1 m intervals.

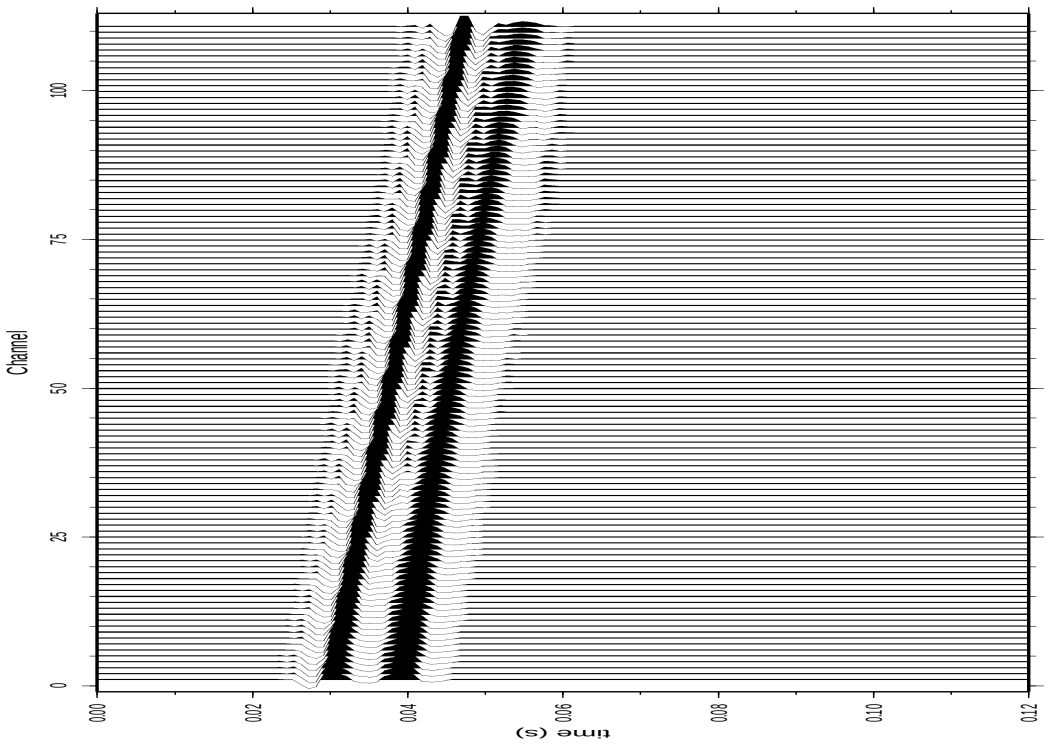

FIG. 13. Shot 50 out of 111, simulated via a frequency domain finite difference method.

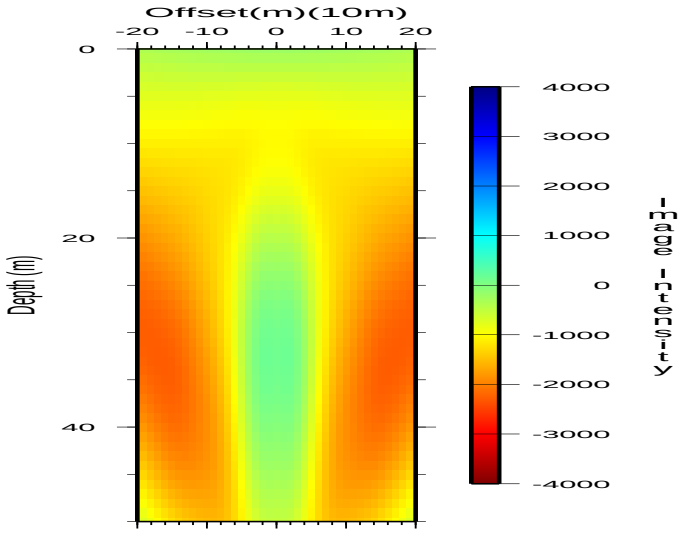

FIG. 14. Horizontal offset image gather at the location of the reflector in Figure 12.

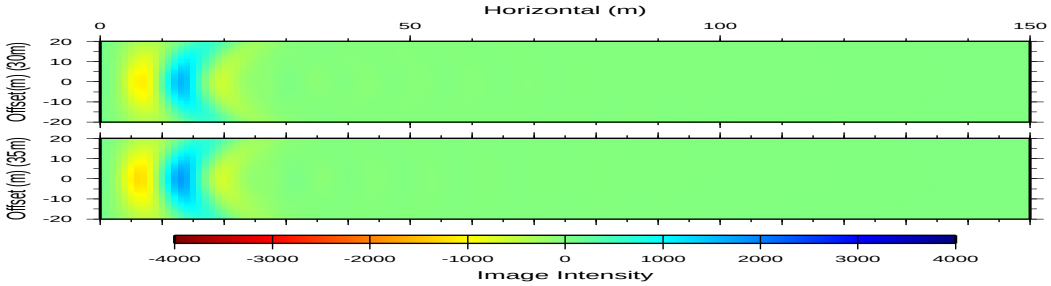

FIG. 15. Vertical offset image gathers at 30, 35 m depth for synthetic data from Figure 12.

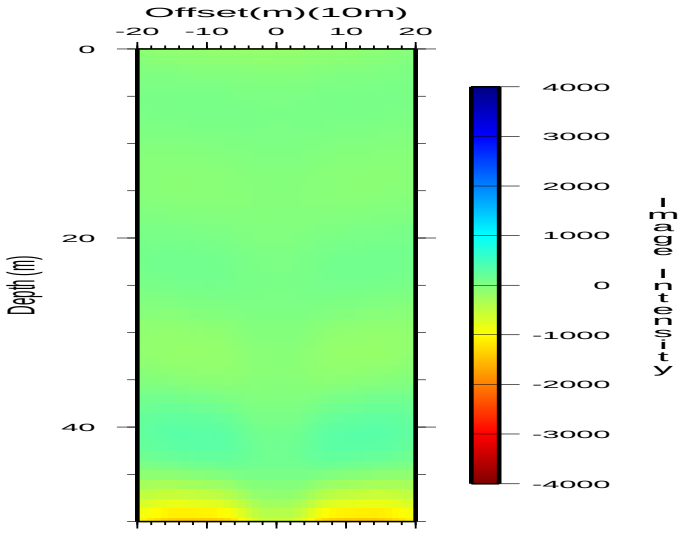

FIG. 16. Filtered horizontal offset image gather at the location of the reflector in Figure 12.

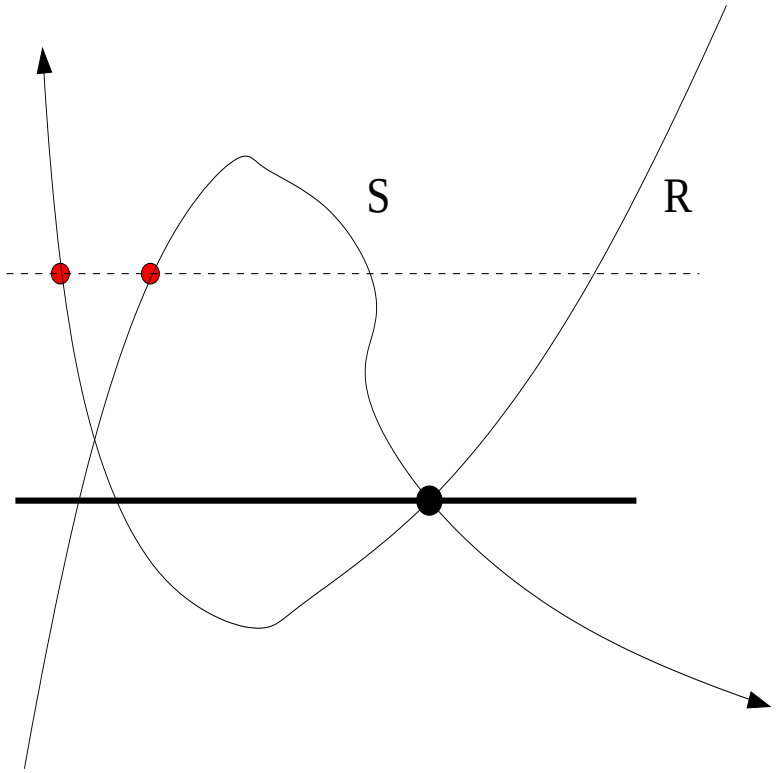

FIG. 17. Cartoon suggesting that zero-offset focussing of restricted offset image gathers may be a local property when rays can turn arbitrarily. The figure is meant to suggest that the generalized image points indicated by the red dots, which are horizontally offset from each other, may have the same total travel time as the physical image point (black dot).